Faculty of Physics
Joint Master Program in Natural Sciences of Agricultural University of Georgia and Free University of Tbilisi

Master Thesis

Monte Carlo Simulation for the JEDI Polarimeter Performance

Mariam Abuladze

Supervisors:
Prof. Dr. Zaza Metreveli
Dr. Irakli Keshelashvili
Advisor:
Dr. Giorgi Macharashvili

October 31, 2019
Tbilisi, Georgia

Contents

1 Introduction **3**
- 1.1 Physics Motivation . . . 3
- 1.2 Electric Dipole Moment . . . 4
- 1.3 EDM Search in Storage Ring . . . 5
- 1.4 Polarization Measurement . . . 7
- 1.5 COSY accelerator facility . . . 8

2 JEDI Polarimeter concept **10**
- 2.1 Vacuum Modules . . . 11
- 2.2 The target . . . 11
- 2.3 The detector . . . 13

3 The Polarimeter Model in GEANT4 **15**
- 3.1 Basic Concept of GEANT4 . . . 15
- 3.2 General Scheme of the code . . . 15
- 3.3 Polarimeter Geometry description in GEANT4 . . . 17
- 3.4 Event Generator for the Simulation . . . 20

4 Primary test of new GEANT4 model **23**
- 4.1 Validation of MC code . . . 23
- 4.2 Maximum effect of target position on forming asymmetry . . . 25
- 4.3 Average effect of target position on forming asymmetry . . . 28

5 Background caused by detector parts **30**
- 5.1 Geometry of symmetric volumes in sumulation . . . 30
- 5.2 Analysis of obtained data . . . 31

6 Asymmetry Related to a Beam Vertical Position **33**
- 6.1 Asymmetry without Target Material . . . 34
- 6.2 Asymmetry with Target Material . . . 36

7 Summary **40**

8 Appendices **43**
8.1 Appendix 1 43
8.2 Appendix 2 44
8.3 Appendix 3 46
8.4 Appendix 4 47
8.5 Appendix 5 48

9 Acknowledgements **52**

Chapter 1

Introduction

1.1 Physics Motivation

One of the most challenging issues in Physics is the dominance of matter over antimatter in the Universe. The Standard Model (SM) of Particle Physics, invented in 1960s, describes the origin of elementary particles and the interaction between them [1]. Symmetries are the fundamental concepts in modern Physics and the three of them, defined in SM, will be discussed below [2].

The Parity symmetry (P) is a symmetry when the Physical processes develop equally if spatial coordinates are inverted with respect to origin of the coordinate system. The Parity symmetry is denoted as P. The Charge symmetry (C) is a symmetry under charge conjugation and it is violated if a particle and antiparticle interaction with environment is different. The third one, the Time symmetry (T) violation takes place when particle acts in a distinguished way in the reverse of time [2]. Consequently, if we discuss regarding symmetry violation, it means that Lagrangian is not invariant under certain transformations, three of which are defined above.

According to the SM, explanations for disappearance of antimatter in early universe is based on the assumption that these fundamental symmetries are violated [3]. In compliance with the theorem by G.Lueders and W.Pauli, the combined CPT symmetry is kept in all physical processes unchanged in the SM [4, 5]. On the other hand, it is experimentally revealed that T symmetry is violated, thus CP should also be violated to keep CPT symmetry and vice versa [2].

CP violation sources in SM is not enough to explain the value of such difference between the amount of matter and antimatter in the universe [3] as one of the possible arguments for breaking of CP invariance is the existence of non-vanishing Electric Dipole Moment (EDM) of baryons [6], which according to SM is almost zero (below experimental limit 10^{-27}) [7].

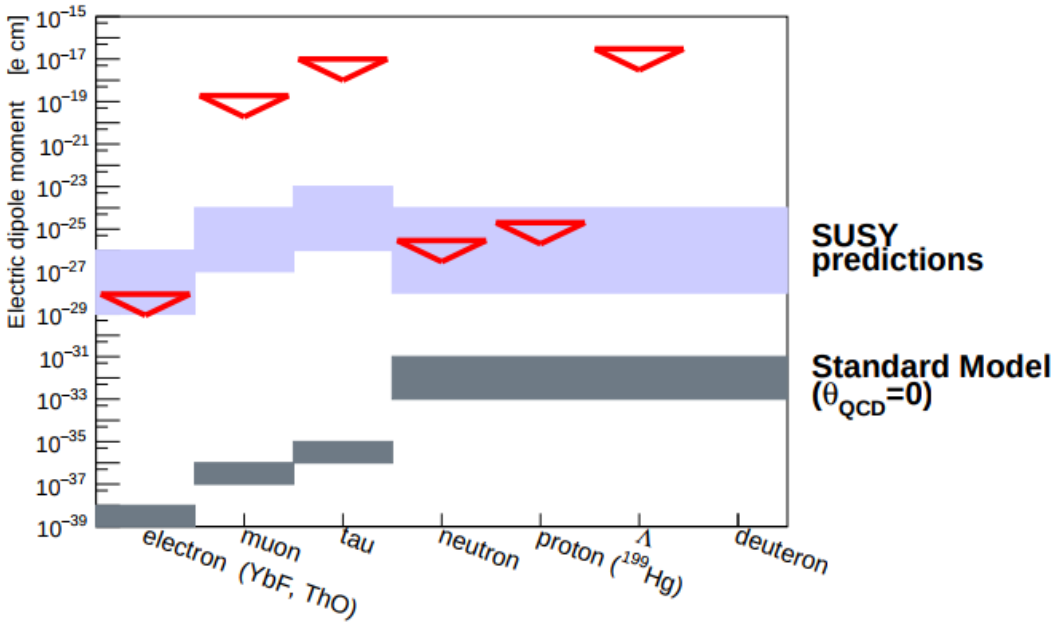

Figure 1.1: EDM predicted by SUSY and SM and current experimental limits.

Such interest in EDM is generated by the fact that tiny non-vanishing EDMs of elementary particles is predicted by SM [8]. The difference between EDMs of elementary particles predicted by SM, Super Symmetry (SUSY) and current experimental limits (with red marks) is displayed on the chart in Figure 1.1[9].

For example, neutron EDM is 10^{-31} - 10^{-31} $e\,cm$, while electron EDM equals 10^{-40} and muon EDM amounts to 10^{-38} $e\,cm$. However, there are theories beyond Standard Model which provide EDMs that are several orders higher, such as SUSY model in which neutron EDM is of order 10^{-26} - 10^{-29} $e\,cm$. [7] Consequently, the measurement of EDM gives a possibility to evolve Physics beyond SM.

The existence of permanent electric dipole moment of charged particles, which is a fundamental feature for all of them, makes the foundation for Juelich Electric Dipole moment Investigation (JEDI) collaboration [9]. Up to now, all measurements of EDMs are comparable to zero [9]. Together with neutral particles, EDMs of charged particles, like protons and deuterons, are the subject of interest to search all sources of CP violation [10].

1.2 Electric Dipole Moment

Electric Dipole Moment in classical Physics is defined by charge distribution in volume and calculated by the formula:

$$\vec{d} = \int \vec{r}\rho(\vec{r})d\vec{r} \tag{1.1}$$

According to the definition, the spin direction is parallel to EDM:

$$\vec{d} = \eta_{EDM}\frac{q}{2mc}\vec{S} \tag{1.2}$$

in which $\vec{d}$ is EDM and $\vec{S}$ is a spin of a particle.

The EDM is considered to violate P and T symmetry. If an elementary particle is located in uniform and parallel electric and magnetic fields, the Hamiltonian of the system is:

$$\vec{H} = \vec{\mu}\vec{B} + \vec{d}\vec{E} \tag{1.3}$$

P transformation should not change electric field and respectively, the T transformation should not alter magnetic field, however, they change these fields. But in case of C transformation, the direction of all vector quantities included in Hamiltonian are reverted and thus, Hamiltonian is conserved. It means that EDM violates T and CP symmetry, thus CPT symmetry is maintained.

The EDM of a particle is a fundamental feature of all elementary particles [11]. Subatomic particles with non-zero spin can only have fixed EDM [3] providing that T and P symmetries are violated while charge (C) symmetry is maintained [2]. Thus, it is the quantity which should be measured in the experiment.

Up to now experiments for neutral systems like neutrons, atoms and molecules have been conducted [9]. The current experiment is supposed to use the storage ring to measure EDM of charged particles, Deuterons [10].

1.3 EDM Search in Storage Ring

As it is mentioned in Section 1.1, EDM is the candidate of CP violation sources, which explains matter-antimatter asymmetry. In order to enable EDM to be measured for charged, elementary particles, experimental methods are investigated within JEDI collaboration [9].

General methodology is based on using a storage ring, an accelerator in which a beam of particles circulate for a long period of time, for hours, and radial electric field or vertical magnetic field can be applied [13]. Polarized particles or atoms are trapped along the storage ring, each of which has defined energy and spin directed to an impulse vector in the laboratory frame [14]. The ring is designed to maintain such polarization for approximately 15 minutes [14]. It is called spin coherence time.

Due to EDM coupling with radial electric field, the polarization of particles is constantly changing in relation to an impulse vector. The change of polarization direction is the key point for measuring EDM [15].

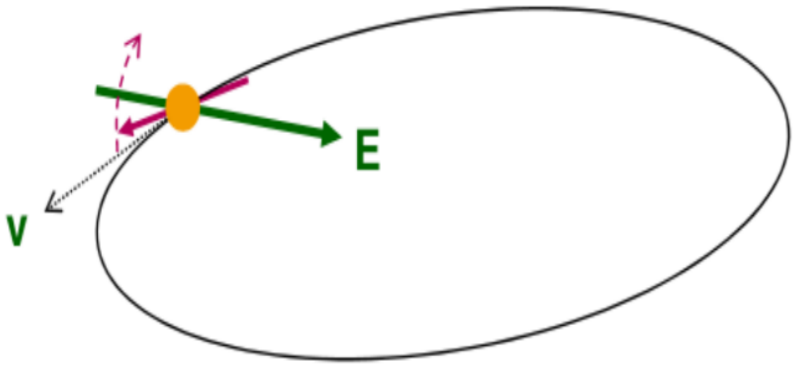

Figure 1.2: EDM coupling with electric field

The Figure 1.2 represents the EDM signal for a charged particle in a storage ring, which is similar to the model described in [14, 15]. The purple arrow is a spin vector of a particle which initially is aligned along an impulse vector. Because of the interaction between the EDM of a particle and the inward electric field, the spin starts precessing in the vertical plain, which is orthogonal to the plain of the ring. A particle in a storage ring feels both magnetic and electric fields in its rest frame, thus its spin precession will be modified by the presence of an EDM [14]. Therefore, after the injection a longitudinally polarized beam in the storage ring, it is possible to detect the EDM signal by observing the increase of the vertical polarization due to EDM interaction with the inward radial electric field in the particle rest frame.

JEDI collaboration aims to design a storage ring which improves systematic and statistical sensitivity of EDM measurement and reach the value of its sensitivity of 10^{-29} e*cm [16, 17].

The search for permanent EDM of elementary particles is of fundamental scientific importance, since a finite EDM would indicate the violation of T invariance. The equivalent CP violation is one ingredient of the so-called Sakharov conditions required to explain the apparent matter-antimatter asymmetry of our Universe [1]. EDMs may thus resolve the puzzle of our existence[7]. No EDM has been observed to date [18]. A new idea, promoted at Forschungszentrum Jülich, is to search for EDMs of charged particles (protons, deuterons) in novel precision storage rings [9, 10].

1.4 Polarization Measurement

The polarization of the beam of particles is defined as the average of the each individual particle's spin. The vector polarization along Y axis is defined in the following way:

$$P_y = \frac{N\uparrow - N\downarrow}{N\uparrow + N\downarrow} = P\uparrow - P\downarrow \tag{1.4}$$

Where $N\uparrow$ is the number of up-polarized[1] particles, $N\downarrow$ is number of down-polarized[2] particles. $P\uparrow$ and $P\downarrow$ are probabilities of finding particles with up and down polarization respectively.

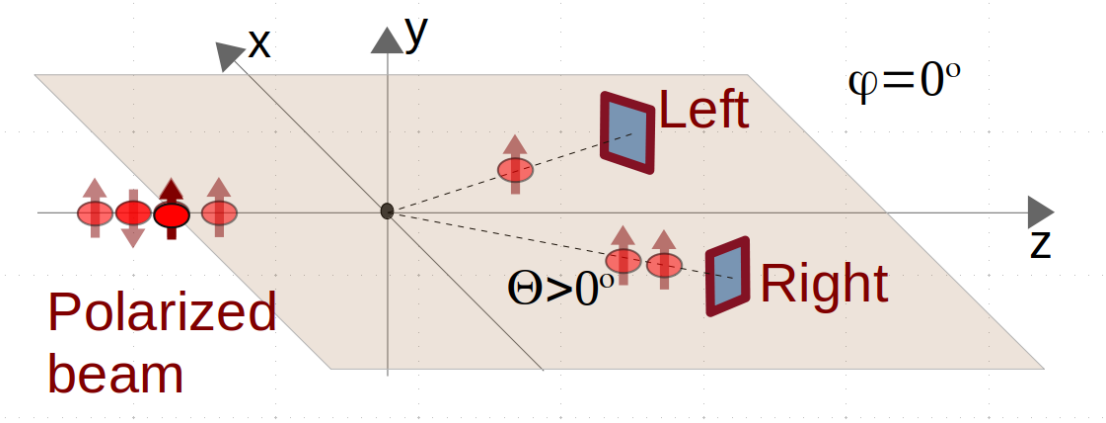

Figure 1.3: Polarization measurement (Experimental technique)

The Figure 1.3 describes the experimental technique for beam polarization measurement [15] and the location of the particles' detector, defines the scattering plain and the direction of the positive Z axis ($\phi = 0^o$). The scattering angle is Θ.

The polarization of deuteron beam can be determined by measuring deuteron-induced reaction rates on a Carbon target, provided that the analysing powers (sensitivities to the polarization) are sufficiently large [21].

$$\sigma^{pol}(\Theta, \phi) = \sigma_0(\Theta)(1 + \frac{3}{2} P_y A_c cos\phi) \tag{1.5}$$

The value $\sigma^{pol}(\Theta, \phi)$ is a differential cross section of Cd reaction. If a beam is not polarized its value is not a function of ϕ, therefore $\sigma_0(\Theta)$ showcases the same for unpolarized beam. P_y is effective polarization along Y axis.

[1]Spin is parallel to positive Y direction
[2]Spin is parallel to negative Y direction

$$P_y = Pcos\phi \tag{1.6}$$

The value measured by the detectors are

$$\frac{N_L - N_R}{N_L + N_R} = P_x A_c(\Theta) \tag{1.7}$$

$$\frac{N_U - N_D}{N_U + N_D} = P_y A_c(\Theta) \tag{1.8}$$

In which $A_c(\Theta)$ is the analysing power of Cd reaction.

For the EDM experiment the large vector analysing power is available due to suitably chosen targets, which make it preferential to concentrate on vector polarization measurement.

1.5 COSY accelerator facility

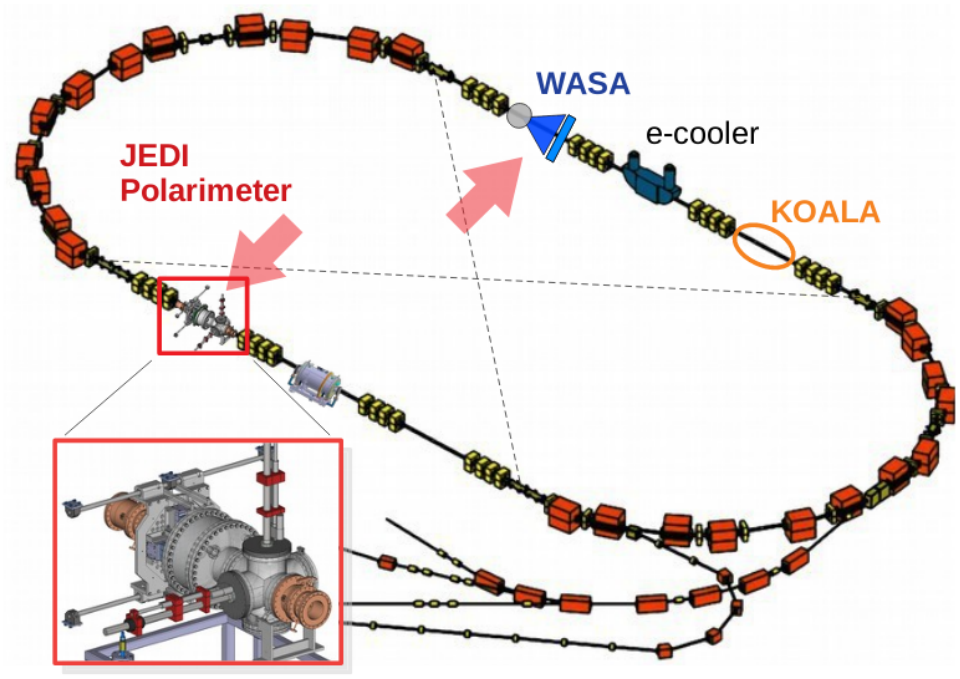

Figure 1.4: COSY with inserted polarimeter

The Cooler Synchrotron (COSY) is located in Forschungszentrum Juelich, Germany [9]. Its graphycal illustration is shown in Figure 1.4, which highlights three parts of COSY[12].

The first part is the source (illustrated in the Figure 1.4) that can produce polarized and unpolarized beam of hydrogen and deuteron ions. The produced ion beams is transferred to an injector cyclotron called Juelich Isochronous Cyclotron (JULIC). This device can increase a kinetic energy of a beam up to $45\,MeV$ for hydrogen and up to $76\,MeV$ for deuteron. From JULIC the beam is transferred to COSY storage ring. COSY can accelerate protons and deutrons to a momentum up to $3.7\,GeV$, which equals kinetic energy of $2.8\,GeV$ for protons and $2.2\,GeV$ for deutrons. COSY accelerator has entire circumference of $184\,m$. The length is occupied by two straight and arc sectors of inner radius $16.5\,m$. (this short description was taken from PHD thesis of Fabian Mueller [12]).

As it is shown in Figure 1.4, an electron cooler (E-Cooler) is available in COSY. Electron coolers are intended to narrow down the interval of particles momentum in order to prolong spin coherence time, which happens by interaction between the beam of positively charged particles and the beam of electrons [18].

Apart from that, we have stochastic coolers the locations of which are displayed by the end points of dash lines in Figure 1.4. Stochastic coolers perform together with diagnostic systems. The diagnostic systems include a beam profile monitor to measure a transverse beam profile. The transverse beam position is measured at several places around the ring by beam position monitors. Stochastic coolers operate with the help of the results from diagnostic systems in order to shorten the range of particles momentum and horizontal distribution of their locations[9].

The measurements of polarization are carried out as the beam circulates the ring. In order to perform experiments in Particle Physics, several internal experimental places, where targets and particle detectors can be installed, are available. Two of them displayed in Figure 1.4 are Wide Angle Shower Apparatus (WASA) and JEDI Polarimeter [9]. Polarization measurement by JEDI polarimeter will be considered in this thesis.

Chapter 2

JEDI Polarimeter concept

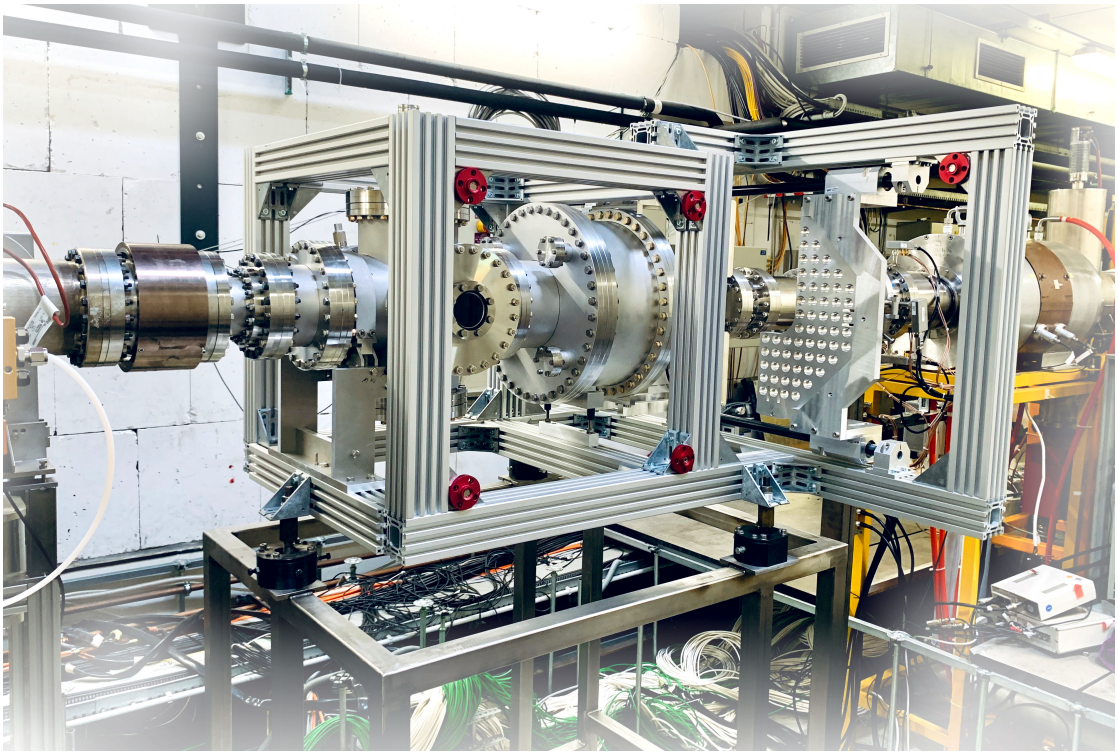

Figure 2.1: JEPO at COSY

The Figure 2.1 represents JEPO at COSY, which consists of three main parts: vacuum modules, the target and the detector. This Chapter explains the parameters of these components and the coordinate system, in the frame of which particles' motion is considered.

2.1 Vacuum Modules

This section is intended to describe the main parameters of vacuum modules of JEDI polarimeter (JEPO). During the experiment polarized beam is used circu-

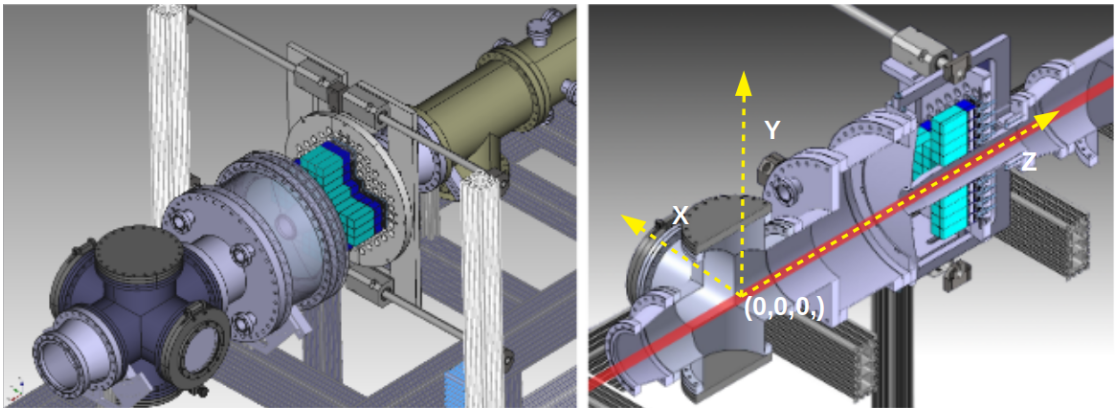

Figure 2.2: construction of polarimeter

lating along the COSY storage ring along the stable orbit. The straight red line on Figure 2.2 represents the beam and Z axis is directed parallel to the beam, the positive direction of which corresponds to the impulse of particles in the beam. The central location of the target and the beam are considered to be at the origin of coordinate system.

The physical dimensions of steel materials, which provide vacuum inside the storage ring is shown in Figure 2.3. Each vacuum module has cylindrical symmetry and all of them together make up the structure of JEPO (Figure 2.2).

2.2 The target

As it is indicated above, in order to measure the polarisation of beam particles should interact with material and be involved in a reaction which has defined analysing power[21]. deutron-Carbon (dC) reaction has very high analysing power (close to 1 at a certain point) so Carbon has been chosen as a target material[21].

The Figure 2.4 represents the virtual model of the polarimeter (Figure 2.2) with a carbon target and the beam inside. It is visible that initially, beam is scattered because primarily, the target was considered to be spotty and the beam makes an impression of primary elastic scattering on such target. However, such target has not been developed for the time being. Actually available carbon target with dimensions $30 \times 30mm \times 20\,mm^3$ in which particles experience multiple elastic

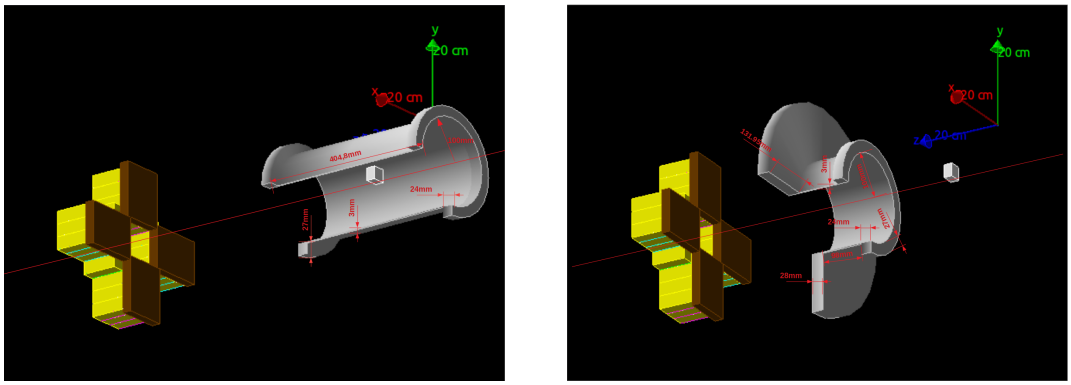

(a) Target Tube

(b) Small Barrel

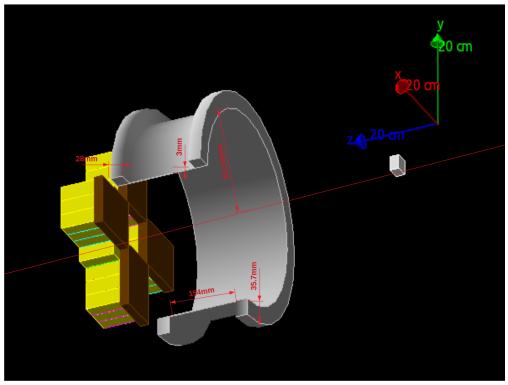

(c) Large Barrel

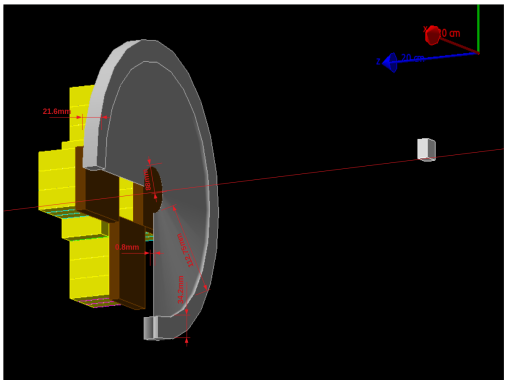

(d) Exit Window

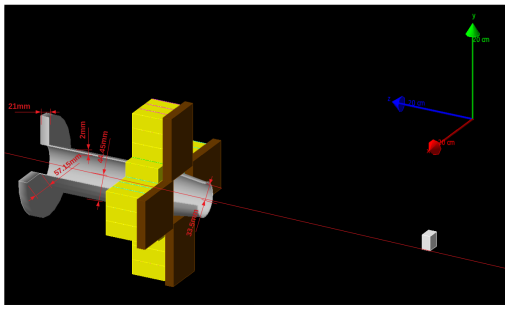

(e) Narrow Tube

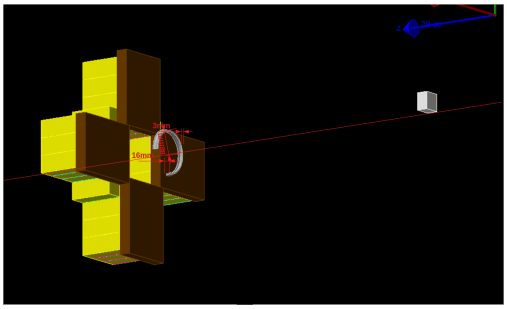

(f) Beam Tube

Figure 2.3: The figure describes vacuum modules with their physical dimensions

scatterings is used. In the simulation the vertical position of the target is altered to evaluate its influence on the asymmetry (Appendix 2). This is one of the crucial goals of the Master Thesis which is described in detail in Chapter 6.

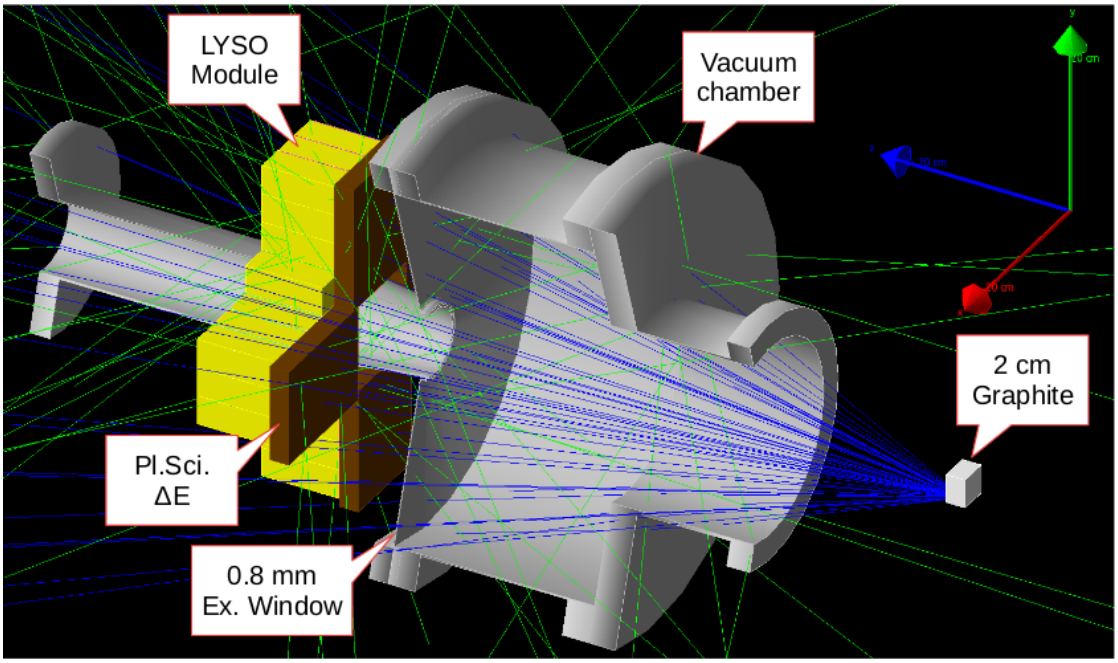

Figure 2.4: JEPO with target

2.3 The detector

This section describes the polarimeter detector components. These components include $Lu_{1.8}Y_{0.2}SiO_5$:Ce (LYSO) crystals and plastic scintillators[12].

The calorimeter, the main part of the polarimeter detector, comprises several LYSO modules. Each module is an independently assembled detector and contains a heavy, fast, radiation-hard and inorganic scintillating crystal LYSO of the size $30 \times 30 \times 100\, mm^3$ and the SiPM[1] photodetectors [12]. The LYSO crystals inserted in the current experimental setup are designed for medium energies up to $350\, MeV$ for deuterons and $300\, MeV$ for protons[12]. In Figure 2.5(b) the front view of the detector is shown. The four rectangular plastic scintillators are placed at the front of the sensitive modules. The Figure 2.5(b) represents the arrangement of LYSO crystal modules. The entire structure of the detector consists of 52 such modules[2], arranged vertically and horizontally (12 modules in one arm) together with four modules in the corners (Appendix 8.1). The Figure 2.3 shows an engineering sketch of constructed detector, where red line refers to the track of the beam. The front surface dimensions of a plastic scintillator is $130 \times 100 \times 10\, mm^3$, while the dimensions of the surfaces of each arm, consisting of 12 modules, is $12.3 \times$

[1] Silicon photomultiplier

[2] *this corresponds to incomplete version of the calorimeter*

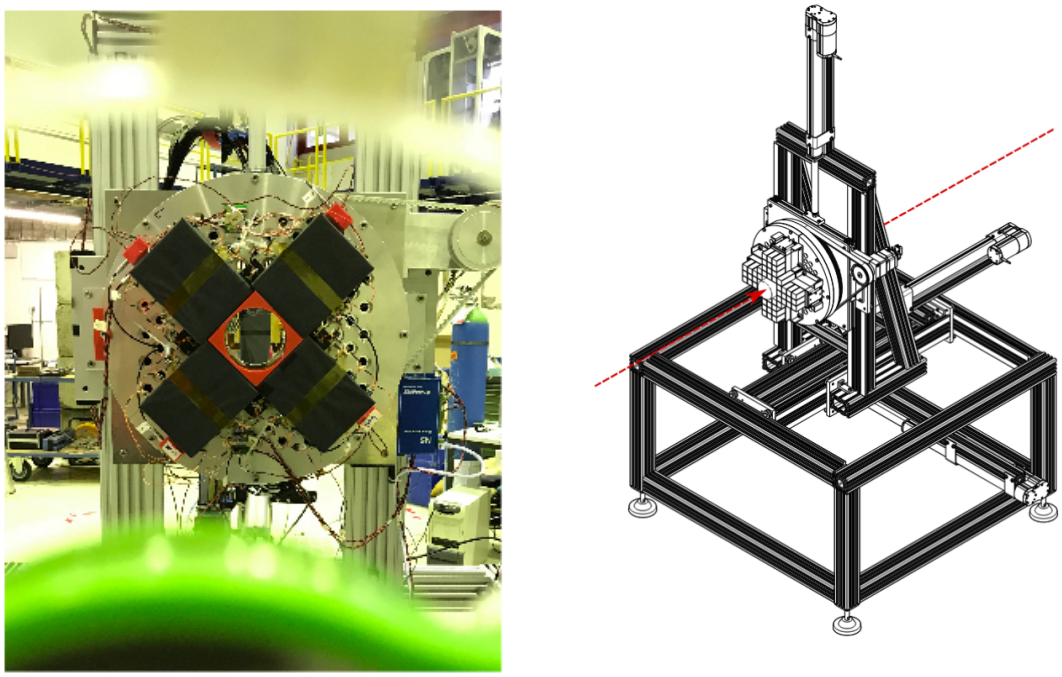

(a) Plastic scintillators in front of LYSO

(b) LYSO crystals

Figure 2.5: The left figure shows the front side of assembled scintillators and the left one illustrates the engineering sketch of a detector

$9.2mm^2$. As a results, the scintillators cover almost one third of the corner crystals (Appendix 8.1).

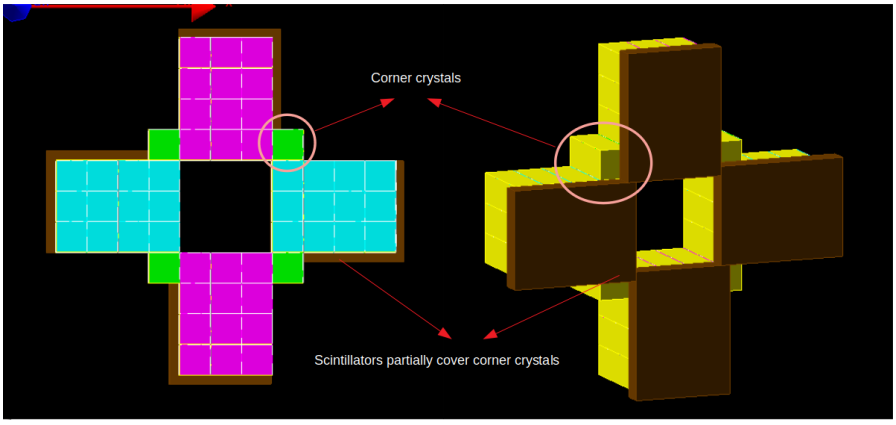

Figure 2.6: Two different perspectives of LYSO crystals and plastic scintillators.

The assembled detector is shown in Figure 2.6.

Chapter 3

The Polarimeter Model in GEANT4

3.1 Basic Concept of GEANT4

GEANT4 is a tool to simulate the passage of a particle through a matter. Its areas of application include High Energy, Nuclear and Accelerator Physics, as well as studies in medical and space science[19]. The simulation considered in this Master Thesis represents interaction of high energy deutrons with steel materials, plastic scintillators and LYSO crystals.

3.2 General Scheme of the code

In High Energy Physics the primary unit of an experiment is an event. An event consists of the formation of primary particles and a detector responds to it. In order to use Geant4 in virtual modelling of such events, users have to define their application based on Geant4 user classes[19][20].

There are three mandatory classes, whose methods should be used in order to conduct a simulation. These are the classes which initiate detector geometry, specify the physics to be used and describe how initial particles are generated. Then, there are five optional classes which control the simulation at various stages. The reduced model of the structure of the code is displayed in Figure 3.1.

main.cc is the main class of the simulation, which retrieves all other classes.

G4UIExecutive.hh checks if a specified session is built or not. If not, it goes to the next step[19].

G4VisManager.cc is initiated in main.cc to perform visualization.

G4MTRunManager.cc creates and starts worker threads.

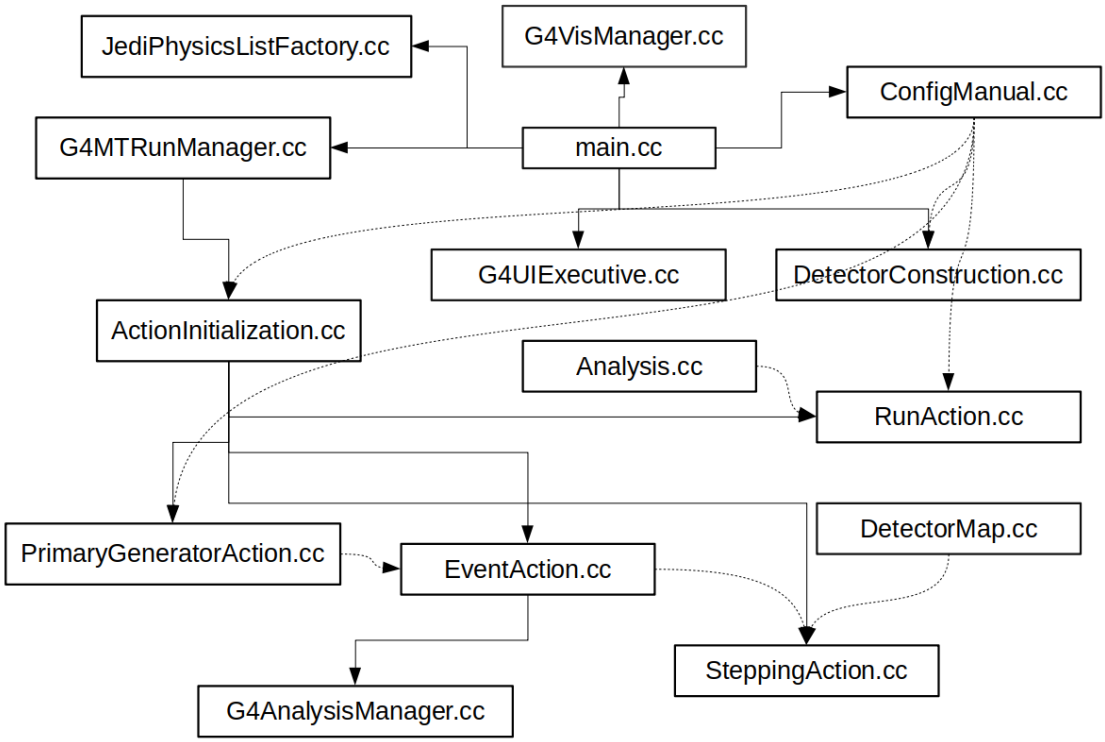

Figure 3.1: Minimised scheme of the code.

JediPhysicsListFactory.cc is implemented by main.cc which defines the Physics built in the simulation.

ConfigManual.cc is operated by main.cc and is intended to read a configuration file, written by a user to define basic parameters of a simulation.

DetectorConstruction.cc is also triggered by main.cc and is responsible for constructing the geometry of a simulation.

ActionInitialization.cc - when the G4MTRunManager.cc class initializes the event by implementing ActionInitialization.cc class object.

PrimaryGeneratorAction.cc generates particles which interact with detectors, and defines their initial position and impulse.

RunAction.cc creates the structure of an output file before an action starts.

EventAction.cc fills the file created by RunAction.cc class.

G4AnalysisManager.cc is used by EventAction.cc to fill the tree structure of an output file.

SteppingAction.cc provides any information about the location and impulse of particles at any moment of the simulation.

DetectorMap.cc is not retrieved by any other class as it represents the list of detector names and identity numbers.

Analysis.cc includes necessary root libraries for a GEANT4 code.

That state-of-art of MC simulation, represented in this Master Thesis is a simulation created by Hoyong Jeong (hyjeong@hep.korea.ac.kr) in November, 2017. The simulation used several libraries written by P.maanen in 2016-2017, which are mostly intended to define the features of particles and materials included in GEANT4 model. In the frame of this Master Thesis several modifications in geometry and motion of particles were made. In this process several libraries written by G.Macharashvili on January 23^{rd}, 2015 in Dubna were added.

3.3 Polarimeter Geometry description in GEANT4

The first and most important modification was in LYSO crystals setup. The Figure 3.1 illustrates these changes. In the current GEANT4 model we have 52 LYSO crystals (arranged in a way described in Section 2.3) instead of 124 LYSO crystals as we have in Figure 3.2(a). This change was appropriate for the current experiment as it intends to measure the energy deposited to symmetrically arranged detectors to measure asymmetry (Appendix 2).

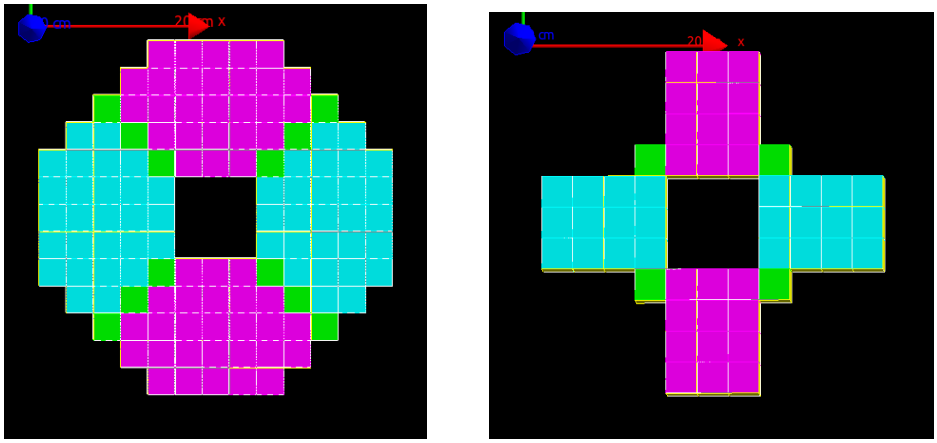

(a) Previous configuration (b) New configuration

Figure 3.2: (a) shows the detector setup in Hoyong Jeong's model (2017) and (b) shows the detector setup in the upgraded model.

The second modification refers to a plastic scintillator in front of detectors. The changes are illustrated in Figure 3.3. As it is displayed, one circular scintillator which fully covers the front sides of LYSO crystals, is replaced by four rectangular scintillators (Figure 2.5(a)) made of the same material.

These changes were needed as circular plastic scintillator has an impact on the spectra of crystals surrounded by black circle in Figure 3.4. It covers one side

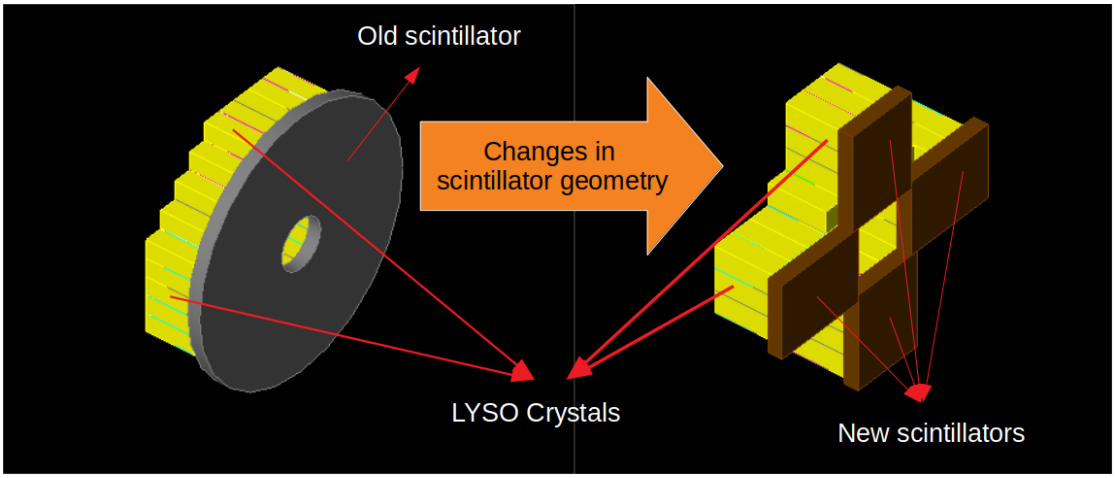

Figure 3.3: Changes is scintillator geometry.

of the detectors located in the corners more than middle detectors. That is why more particles for corner detectors are going through scintillators than for middle detectors. The resulted spectra are shown on the left side of Figure 3.4. The spectrum in blue refers to a corner crystal and the spectrum in red applies to a middle crystal.

The double peak on the spectrum coloured in red is caused by the fact that some particles which were detected by the middle crystal lost their energies in the scintillator. This effect appears only for certain detectors, while fully unpolarized beam is considered, so it is the flaw of the current virtual model.

However, there is not full coincidence between dimensions of LYSO crystals and plastic scintillators (see Section 2.3). As a result, there will be a double peak in the spectrum of Corner crystals (Appendix 8.1).

In the event of the results shown in Figure 3.5, beam with 1 million particles with initial kinetic energy of 270MeV was considered. A spectrum of one of the corner crystals is displayed in Figure 3.5(b). There is a couple of peaks - the first with the energy of 250MeV and the second with 270MeV. The first peak corresponds to particles which lost a part of their kinetic energy in scintillators (20MeV) before their being detected by LYSO crystals. The second peak conform to the particles which have not crossed the scintillator and convey all their energy to LYSO crystals.

The next modification of the code was the addition of symmetrical steel modules to the graphical model of the simulation (see section 2.1), which in the real experiment provides vacuum inside the storage ring.

Another essential point for the simulation is the shape and dimensions of the target. The ring target was replaced by a rectangular one (see section 2.2) to

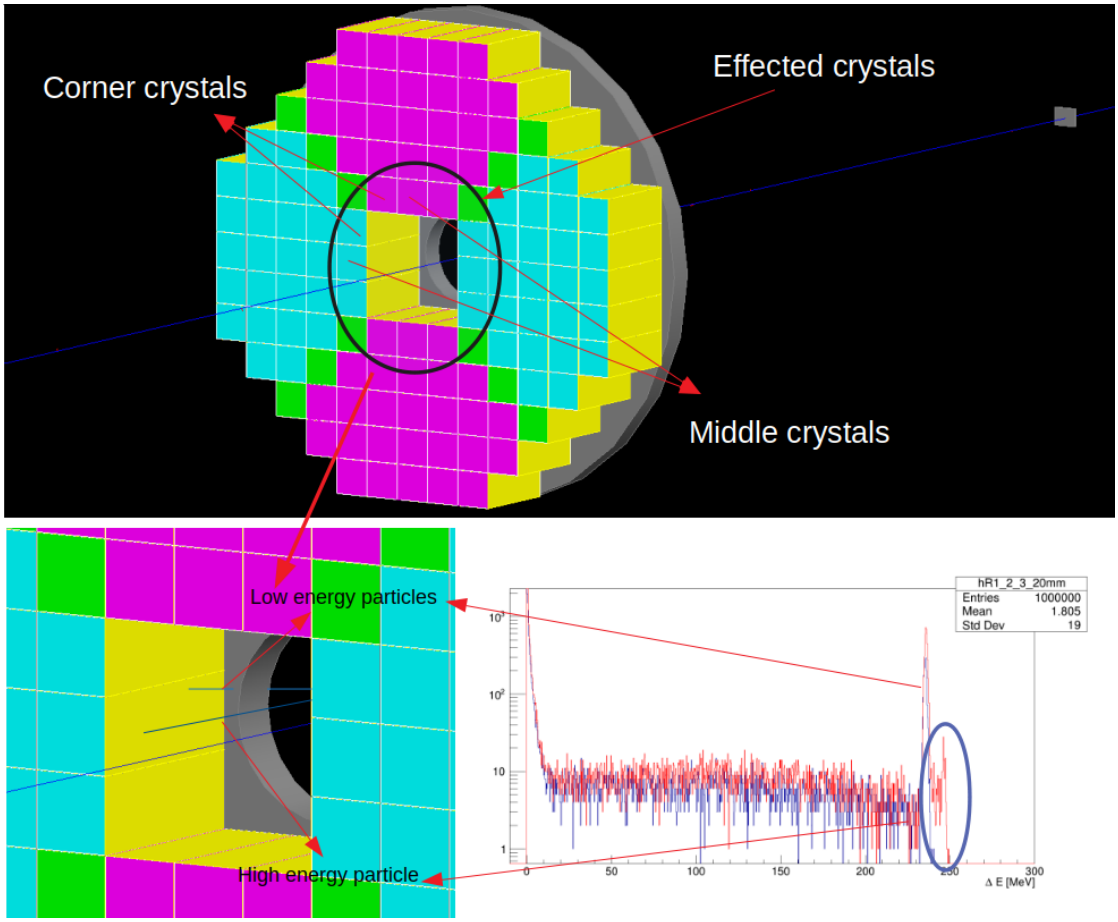

Figure 3.4: Influence of circular scintillator on spectrum of middle crystal.

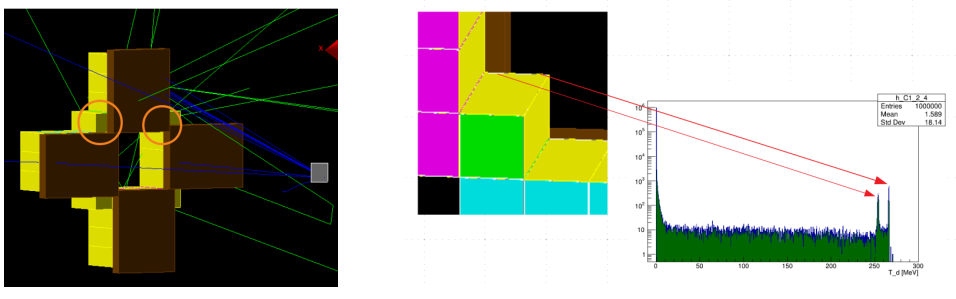

(a) Geometry (b) Spectra

Figure 3.5: (a) Shows geometry of the scintillators and LYSO crystals and (b) displays the double peak in the spectrum of corner crystals caused by the dimensions of rectangular scintillators.

investigate its effect on the ultimate results more precisely.

3.4 Event Generator for the Simulation

For the subsequent development of the code the PrimaryGeneratorAction.cc class (see section 3.2) has been upgraded in order to change the way particles are generated.

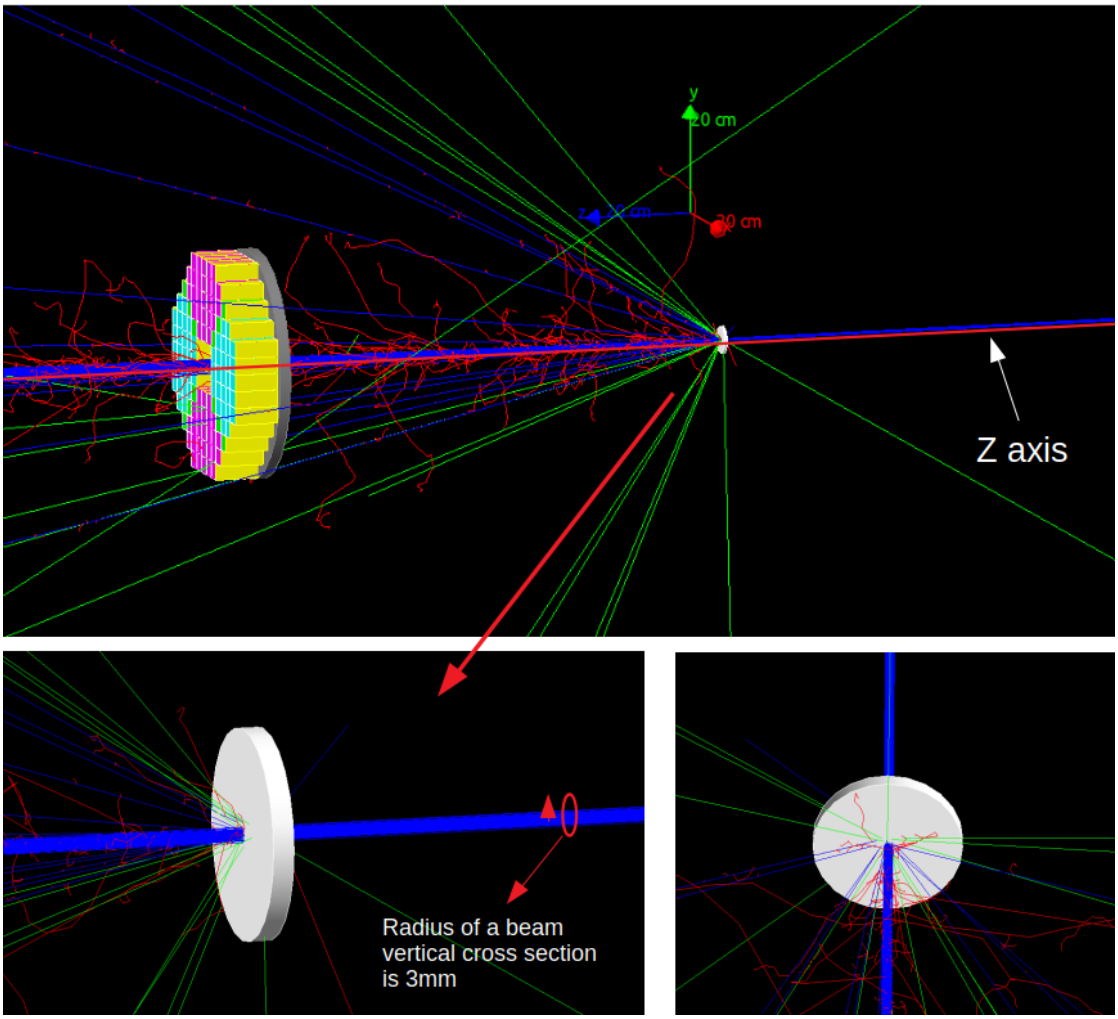

Figure 3.6: Particle generator geometry in GEANT4 model of 2017.

The Figure 3.6 illustrates the particle generator in the older version of GEANT4 model. In the previous model all particles had initial kinetic energy of 270MeV and their momenta were directed parallel to Z axis.

Hence, all particles in the beam move on parallel lines before they interact with the target, but their initial positions differ. As in the real beam particles have non-negligible physical size, the trajectories of some of them are shifted from Z axis. In the particle generator of GEANT4 model this is visualized by random (Gaussian function) distribution of particles initial separation from Z axis and the maximum separation is 3mm. The area in which the points of particle formation are randomly distributed is marked with a red circle in Figure 3.6.

The Figure 3.7 describes the geometry of particle generator in the new GEANT4 model.

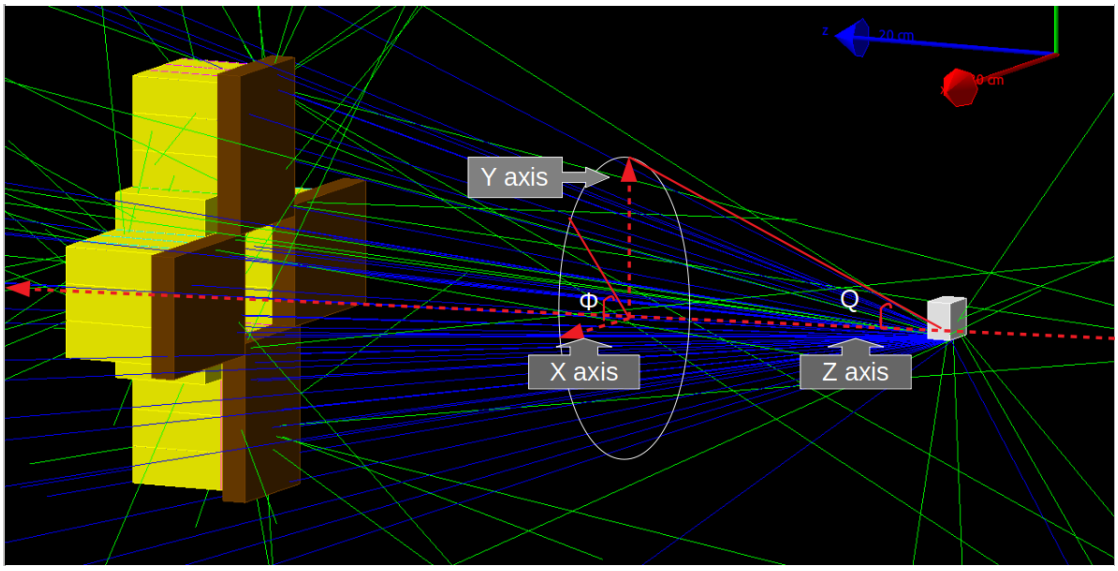

Figure 3.7: Particle generator in the modified GEANT4 model.

In the new version of GEANT4 simulation all particles generate at one point, however their momenta do not have the same direction. They are distributed as a function of ϕ and θ (Figure 3.7). This distribution is needed to visualise the effect of primary elastic dC scattering. The distribution of the momentum direction as a function of θ is always uniform, while ϕ defines polarisation. If ϕ has a uniform distribution we have no polarization. In the current version of GEANT4 simulation the distribution of ϕ is given by the following formula:

$$f(\phi) = c(1 + Acos\phi) \tag{3.1}$$

In which c is normalization constant and A is polarization of a beam. Polarization is given by the formula:

$$A = \frac{N_+ - N_-}{N_+ + N_-} \tag{3.2}$$

N_+ is the number of particles polarised in positive Y direction and N_- is the number of particles polarized in negative Y direction. The index of polarization (A) is defined by a user before launching the simulation.

Chapter 4

Primary test of new GEANT4 model

With all the modifications and additions having done the questions as to how the simulation works for basic cases should be tested.

The first case is measuring an asymmetry when there is a beam and a detector in a geometry without target and vacuum modules which will be discussed in Section 4.1.

The second case will be positioning carbon material target so that it has the maximum possible effect on the formation of asymmetry and investigation its influence on the spectra of different crystals (Section 4.2).

Lastly, the third case will be counting average asymmetry caused by the existence of target in a model. Asymmetry caused by target will be average if there are several beams, each of which is differently influenced (Section 4.3).

The distribution of the direction of deutrons momenta is similar to the one described in Section 3.4. In each case mentioned ten million events are simulated with 270MeV of deutrons initial kinetic energy.

4.1 Validation of MC code

Firstly, in order to check whether simulation works properly and errors caused by numerical methods is negligible, the event of entirely unpolarised beam which flows in the vacuum without carbon target inside is being considered. In this case no asymmetry (Appendix 8.2) is expected to be traced. Thus, the one which might be revealed may be considered as an error of the simulation.

The Figure 4.1 showcases the graphical model of the simulation. There are no vacuum modules and the particle generator lies on Z axis (Figure 2.2).

Figure 4.2 illustrates the results of the simulation. The histograms on the left

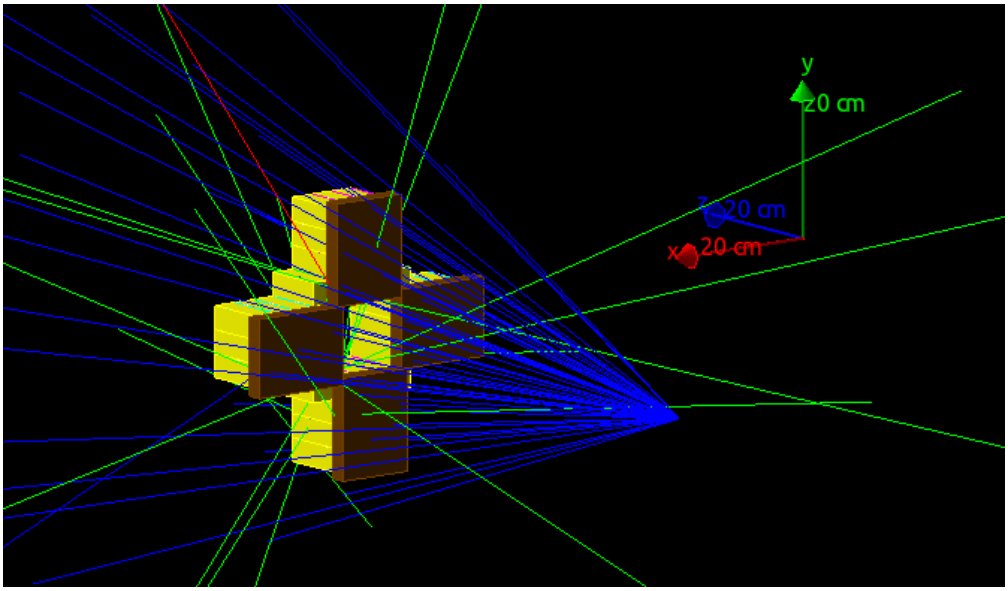

Figure 4.1: All particles move in the vacuum and are detected by LYSO crystals without being interacted with any steel materials.

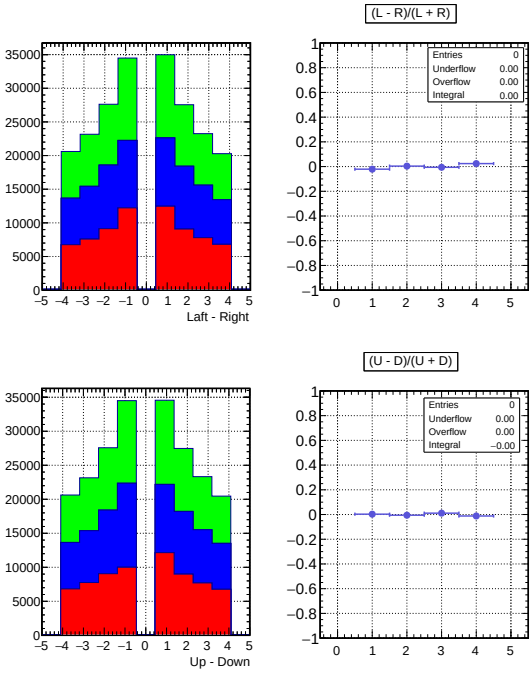

Figure 4.2: Asymmetry between oppositely arranged crystals when there is no target material.

side shows the number of particles detected by each crystal and histograms on the right side shows the difference between the values of symmetrically arranged columns of the right histograms (Appendix 8.2).

It is apparent that asymmetry in energy transfer between Up-Down and Left-Right (Appendix 8.1) crystals is comparable to 10^{-2}. In addition for both directions the relative imprecision of asymmetry which is 0.03 in this case is more than detected asymmetry. Thus, we have no asymmetry without target and vacuum modules if the beam position is not shifted to the vertical direction.

4.2 Maximum effect of target position on forming asymmetry

As the next step, the maximum possible effect of a carbon target positioned forming asymmetry should be estimated. The Figure 4.3 illustrates positioning of target material relative to the beam. All particles are generated behind the target at a lower edge. This way, half of deutrons in the beam go through a target and cross the longest possible distance inside it, thus they lose the greatest possible kinetic energy.

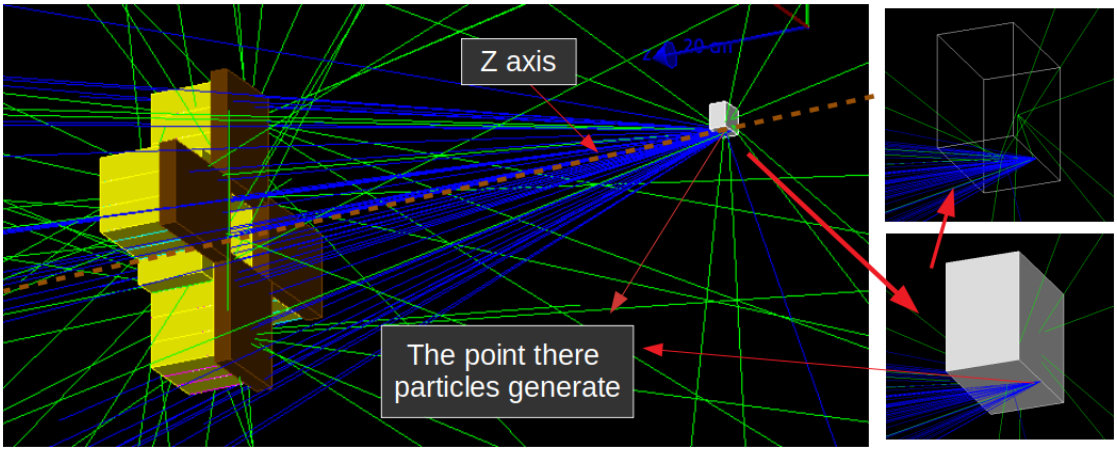

Figure 4.3: Beam and target positioning

Consequently, as the target is shifted to Y direction, (Figure 2.2)there will be no asymmetry between Right and Left crystals, whereas there will be maximum asymmetry between Up and Down crystals (see Appendix 8.1).

As Figure 4.4 illustrates, asymmetry between Up and Down crystals is ten times more (approximately -0,14) compared to the one without target material. These data are of 0.03 imprecision. At the left side of Figure 4.4 there are spectra of U1_2_3 and D1_2_3 crystals (see Appendix 8.5), each of which has a couple of

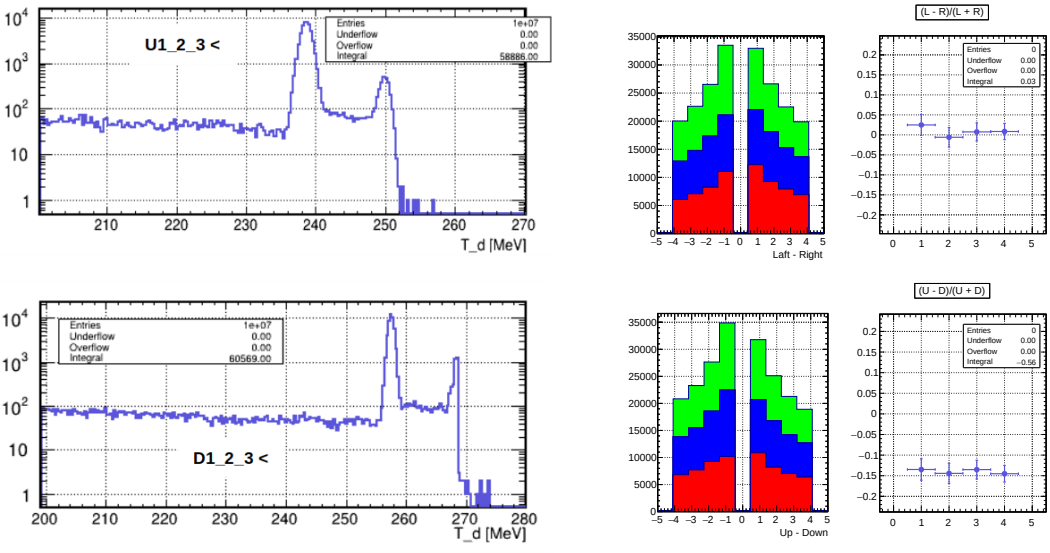

(a) Spectra (b) Asymmetry

Figure 4.4: Asymmetry and spectrum for Up and Down crystals

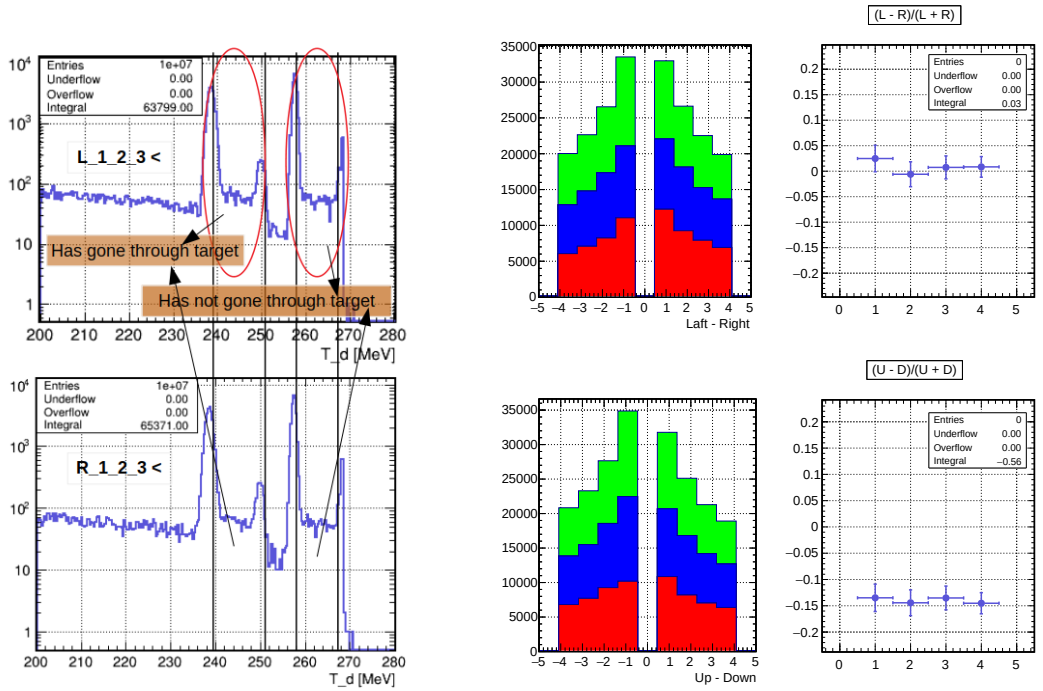

(a) Spectra (b) Asymmetry

Figure 4.5: Asymmetry and spectrum Left and Right crystals

peaks. The low energy (238,5MeV) peak of U1_2_3 refers to the particles which cross the target and plastic scintillator, while high energy peak refers (250MeV) to the ones which cross only the target. The low energy peak for D1_2_3 refers to particles which go through plastic scintillators and high energy peak refers to the ones which go through the vacuum. So particles lose 20MeV of their kinetic energy due to the target material.

Figure 4.5 describes spectra of L1_2_3 and R1_2_3 crystals and asymmetry. It is visible that asymmetry between Left and Right crystals stays in the range of 0.03 uncertainty, however, they reveal different behaviour.

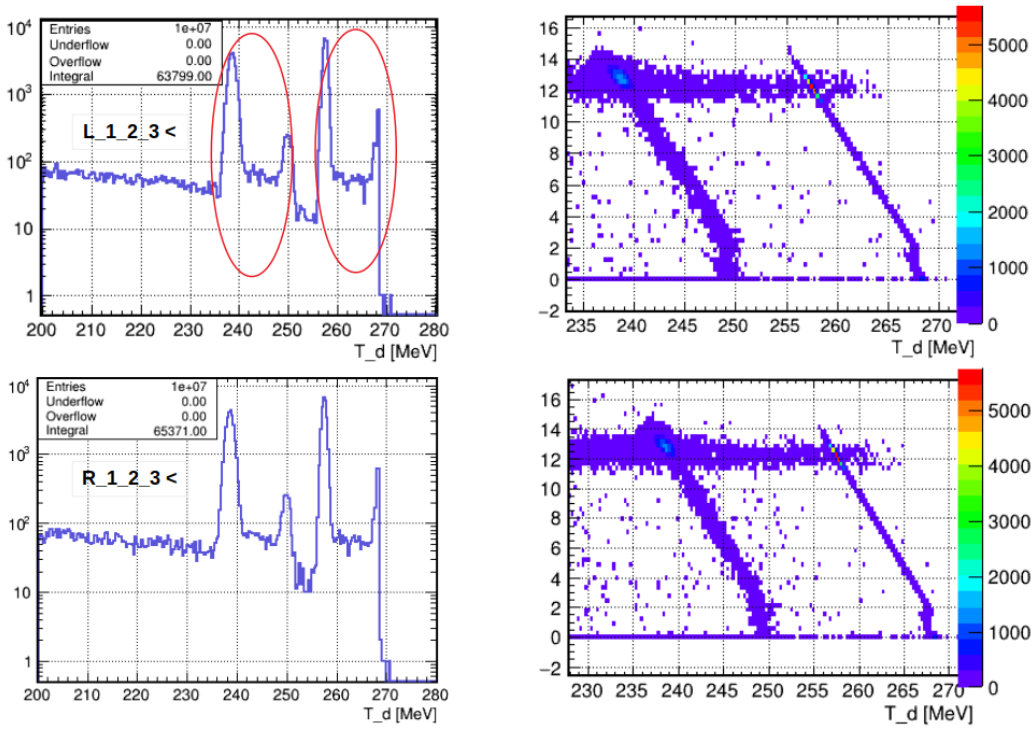

Figure 4.6: The Figure shows two-dimensional analysis of the spectra displayed in Figure 4.5. The horizontal axis of 2D histograms on the left side shows the energy transferred to crystals and the vertical axis shows energy transferred to the scintillator. The corner points of parallelograms on 2D histograms corresponds to the peaks of spectra.

There are two couples of peaks on the both spectra displayed. This can be explained from geometrical point of view. Due to the location of L1_2_3 and R1_2_3 crystals, they detect both particles - those which have crossed the target and which have not. The left red circle on the up-right histogram in Figure 4.5

marks the particles which have gone through the target and the right one refers to particles which have not. The difference between their kinetic energies is again 20MeV, while the energy loss due to the scintillator is almost 10MeV.

4.3 Average effect of target position on forming asymmetry

In this section of the simulation the target is once again shifted along Y axis as it is shown in Figure 4.2. Nevertheless there are several points of particle formation. Neutrons are fired from below the edge of the target at intervals of 2mm along its full length (20mm) parallel to Z axis(see Figure 4.7).

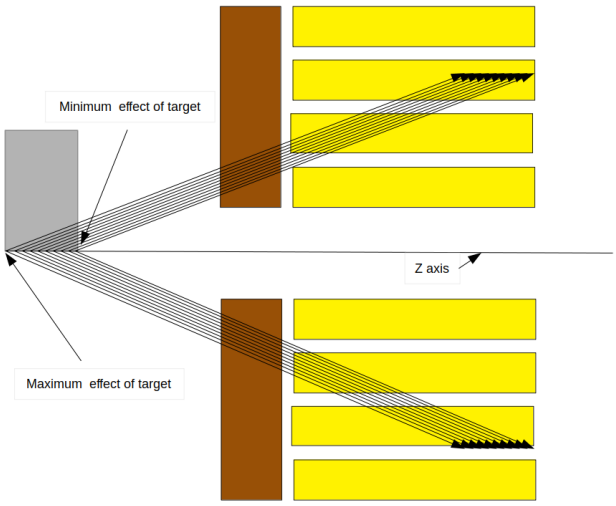

Figure 4.7: Particle generator positioning

The Figure 4.8 describes the results. The asymmetry formed in the case shown in Figure 4.7 is less than the one in the case when there is only one point of particle formation(-0.14). As some particles are shot from the front part of the target, they are less influenced, therefore they generate less asymmetry than those from back sides (Figure 4.7).

The spectra of energy experienced by different LYSO crystals are shown in Figure 4.8. It is noticeable that there is difference between peaks in the spectrum of U_1_2_3 and each of them corresponds to different position of particle shoot. As energy increases, the resolution for each peak rises as well. This fact can be explained by the process experienced by particles in the target. The longer way they travel inside the target, the more unpredictable it becomes how much energy

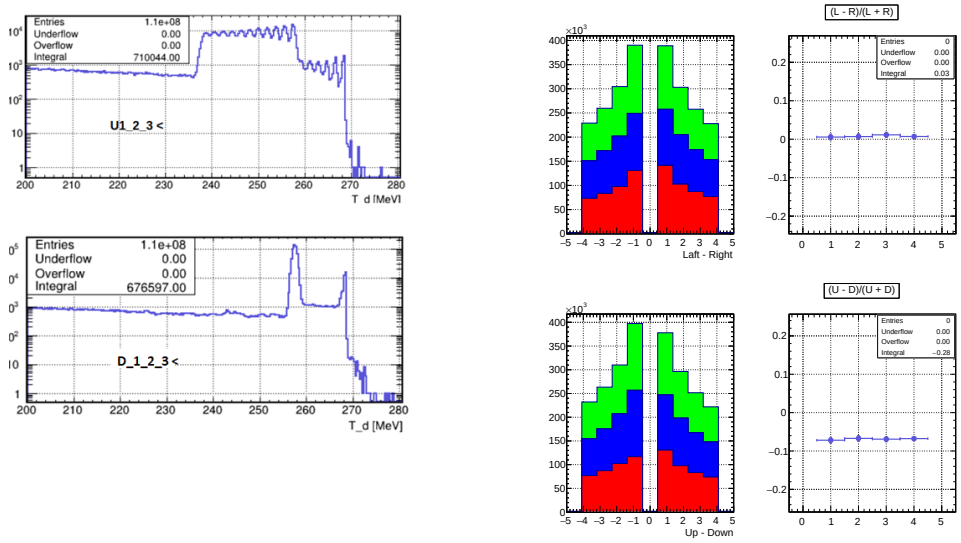

(a) Spectra (b) Asymmetry

Figure 4.8: Average asymmetry between U1_2_3 and D1_2_3 crystals

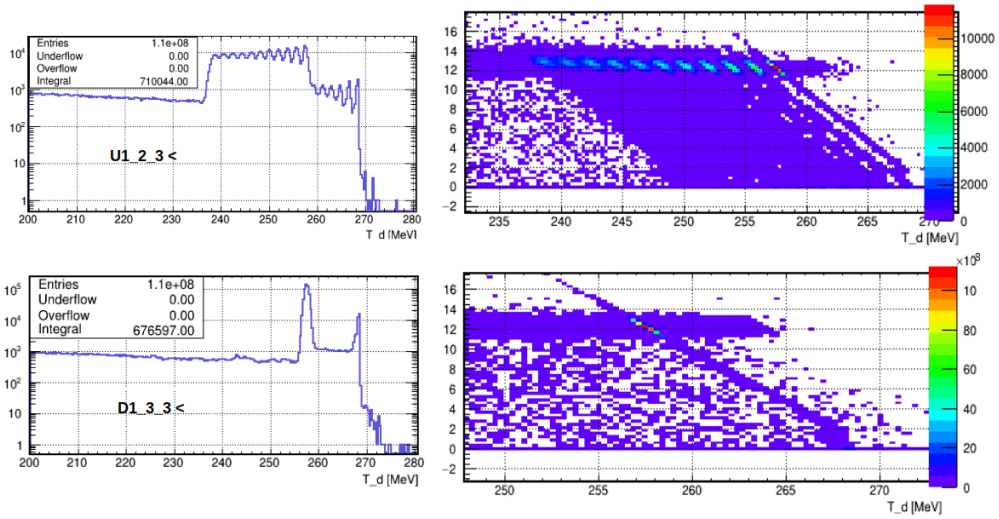

Figure 4.9: Spectra (left side) and 2D analyses (Right side). Yellow point on the left 2D histograms corresponds to energy peaks in the spectra of LYSO crystals.

they will have after leaving the target. Yet on average the longer a particle stays in the carbon target, the more energy is transferred to it.

Chapter 5

Background caused by detector parts

5.1 Geometry of symmetric volumes in sumulation

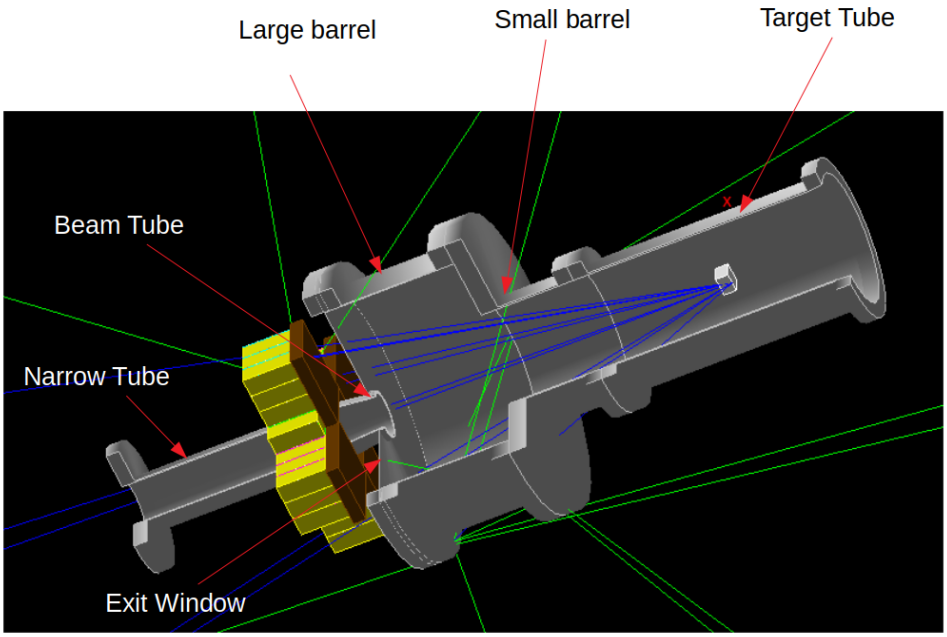

Figure 5.1: Detector geometry with vacuum modules

In a physical experiment vacuum modules (Section 2.1) made of steel material are used to maintain vacuum inside the storage ring which might be related to a

certain background in the spectra.

So the influence of this background on asymmetry, measured in the cases mentioned in Chapter 4, will be investigated in this part of the thesis.

There are six symmetric modules located in such a position that some particles will have to cross them after elastic scattering in carbon target (Geometrical description of these modules - Section 2.1). These are: a target tube, a small barrel, a large barrel, a narrow tube, a beam Tube and an exit window(Figure 5.1), each of which is made of steel with density $7.85 * 10^{-3} g/mm^3$.

5.2 Analysis of obtained data

On the grounds of previous calculations, if we do not have any vacuum modules the asymmetry in energy transfer between the symmetrically arranged crystals is 1% on average with uncertainty of 2% (Section 4.1).

The results of the same calculations with vacuum modules are displayed in the three following tables. In the first row of tables the names of vacuum parts which have been turned on during simulation are mentioned and the numbers of rows of Up-Down crystals on the horizontal axis (Appendix 8.1), between which asymmetry is measured, is written.

Table 5.1: asymmetry caused by steel modules

data	**Target Tube**	**Small Barrel**	**Large Barrel**	**Narrow Tube**	**Exit Window**	**All**
Asymm Row1	0.035	0.019	0.00	0.00	−0.015	−0.014
Asymm Row2	−0.005	0.021	0.019	−0.02	0.00	−0.008
Asymm Row3	0.04	0.005	−0.01	0.01	0.015	−0.006
Asymm Row4	−0.01	0.00	0.00	−0.01	−0.01	−0.001
error	0.03	0.03	0.03	0.03	0.03	−0.03

Table 5.1 shows the asymmetries which can be caused by steel modules as target is turned off and beam is positioned at the center of the system (Figure 4.1). From Table 5.1 it is obvious that all these asymmetries stay in range of uncertainty. Meanwhile they are of the same order like in the case when there are no vacuum modules.

Table 5.2 displays how the value of average asymmetry is fluctuated due to the existence of vacuum modules. In this case target and beam positioning was indistinguishable like in Figure 4.3(Section 4.2). The average asymmetry without any of such modules is 0.07 (Section 4.3). Thus, from Table 5.2 it is vivid that the

Table 5.2: Average asymmetry fluctuation due to steel modules

data	**Target Tube**	**Small Barrel**	**Large Barrel**	**Narrow Tube**	**Exit Window**	**All**
asymm Row1	−0.07	−0.075	−0.071	−0.086	−0.068	−0.08
asymm Row2	−0.069	−0.068	−0.068	−0.07	−0.065	−0.06
asymm Row3	−0.067	−0.064	−0.065	−0.075	−0.081	−0.08
asymm Row4	−0.066	−0.076	−0.069	−0.076	−0.072	−0.115
error	0.01	0.01	0.01	0.01	0.01	−0.01

fluctuation resulted from symmetric volumes is negligible and stays in the range of uncertainty.

Table 5.3 shows fluctuation in maximum asymmetry (Equation 1.4 and 1.5) caused by vacuum modules. In this case target and beam positioning is similar as it is in Figure 4.6.

Table 5.3: Maximum asymmetry fluctuation due to steel modules

data	**Target Tube**	**Small Barrel**	**Large Barrel**	**Narrow Tube**	**Exit Window**	**All**
Asymm Row1	−0.15	−0.2	−0.168	−0.185	−0.15	−0.15
Asymm Row2	−0.14	−0.16	−0.158	−0.15	−0.149	−0.15
Asymm Row3	−0.165	−0.14	−0.14	−0.125	−0.15	−0.15
Asymm Row4	−0.145	−0.18	−0.18	−0.16	−0.151	−0.26
Error	0.03	0.03	0.03	0.03	0.03	0.03

As it is known obvious from previous calculations (Section 4.3) maximum asymmetry which can be generated by target material is 0.15, which is of the order of current results and stays in its range of uncertainty.

The conclusion to be drawn from Chapter 5 is that the values of asymmetry obtained from the cases considered in Chapter 4 can not be significantly changed by adding vacuum modules in a geometry of the simulation.

Chapter 6

Asymmetry Related to a Beam Vertical Position

As the bunch of particles in real beam has non-negligible dimensions, different particles will go through different trajectories. As a result, asymmetry (Equation 1.4 and 1.5) measured by detectors is affected. The analogue of this process in Monte Carlo simulation can be made by shifting the point of particle generator from Z axis (Figure 2.3).

In this case 11 different points of particle formation are considered, Y coordinate (Figure 2.2) of which varies from 0mm to 10mm with 1mm of separation and ten million events are simulated for each point. For these coordinates both cases are investigated when target is turned on and off (Figure 6.1).

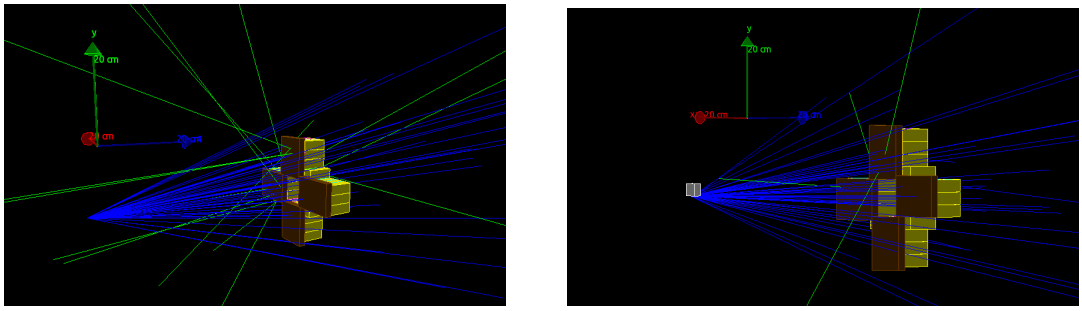

(a) Target is OFF (b) Target is ON

Figure 6.1: (a) shows the position of particle formation and spread when there is no target and (b) shows the same with target material, the position of which corresponds with the beam.

As it is mentioned in Section 3.4, momenta direction of particles have certain distribution as function of θ and ϕ. In this part we have 2 degrees and 22 degrees

upper limit for θ. These are the limits which will not have an influence on the final results (see appendix 8.3).

6.1 Asymmetry without Target Material

In the first part of the chapter the asymmetry caused by shift to vertical position (see Section 2.1) of the beam will be calculated and dependence of asymmetry on the value of a shift will be investigated. In this section both cases when vacuum modules are turned on and off will be considered. Yet, to be more evident, the beam position in Figure 6.2 is displayed without showing these modules. As shown in Figure 6.2, The position of a point of particle formation along a vertical axis varies from 0mm to 10mm, (Figure 2.2) so asymmetry in energy transfer between Up and Down crystals (see Appendix 8.1) is expected.

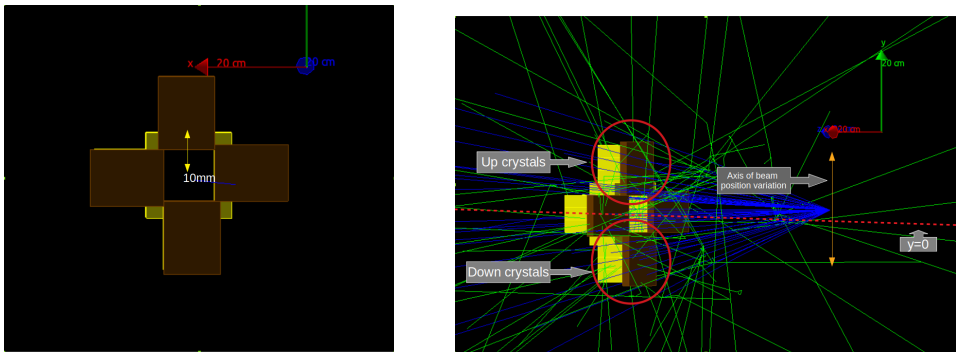

(a) Front view (b) Perspective

Figure 6.2: Beam positioning

The results of the simulation is shown in Figure 6.4.

On the left side of Figure 6.4 the asymmetry when vacuum modules are turned off is displayed, while on the right side the one when vacuum modules are turned on is shown. The horizontal axis of histograms in Figure 6.4 shows a vertical displacements of beam position in millimetres and the vertical axis shows measured asymmetry. The names of histograms indicate the number of rows, the spectra of which are compared (see Appendix 8.1 and 8.2).

It is vivid from Figure 6.4 that when there is no shift in vertical position of the beam, we have no asymmetry, regardless of inserting vacuum modules (this case is checked in Chapter 4 and Chapter 5). However, at the same time, as a beam vertical position increases, the asymmetry increases as well (Appendix 8.1 and 8.2). But this increase has different rates for different rows of crystals. In the case when there are no vacuum modules, the farther a row is from Z axis, the slower the asymmetry increases. For the first rows of Up-Down crystals asymmetry is

0.25 if a beam's Y coordinate is maximum. Then it constantly decreases for the following rows of crystals and reaches 0.14 for the fourth one. This event emerges because the difference between projections of detectors' front surfaces on the plain orthogonal to particles' motion (Figure 6.3) is more important for inner crystals than for outer ones.

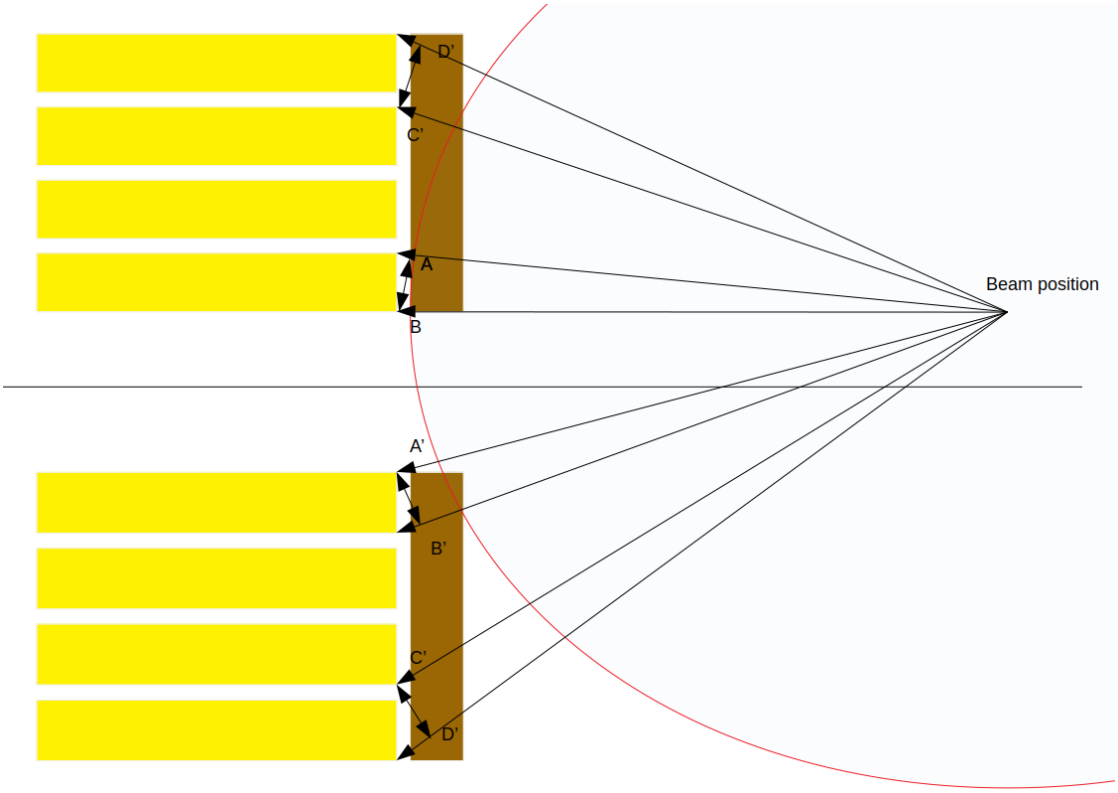

Figure 6.3: Cross section of crystals

However, when vacuum modules are turned on the Row 4 is an exception. As it is vivid from the left column of histograms in Figure 6.4, the measured asymmetry decreases from Row 1 to 3 but increases for Row 4. This effect appears only if symmetric volumes are on, so it might be explained by the fact that when beam's vertical position is shifted, particles interact with vacuum steel modules in a different way. Due to geometrical parameters of these steel materials this effect is more significant for large angles. Thus it makes influence only on the spectra of outer crystals.

6.2 Asymmetry with Target Material

The second part of this chapter refers to the asymmetry caused by vertical positioning of the beam and a target. The rule of beam positioning is the same as it was in the previous section (see Figure 6.5) with target material added. Beam-target system has such a position that in all eleven points of particle formation half of the particles will go through the target and half will not (Figure 4.3). Thus, the target will have the maximum effect.

The Figure 6.6 shows the outcome of the simulation.

Unless there is shift in the vertical position of the beam, there is asymmetry caused by merely target material and it is in the range of -0.14 and -0.16 when there are not any vacuum modules. (This case is considered in Section 4.2 and 5.2).

It is clear from histograms in Figure 6.6 that as a shift to vertical position of the beam increases, asymmetry increases as well. As asymmetry is negative when Y coordinate of the beam is zero. There is one point for each row of crystals (Appendix 8.1 and 8.2) for which asymmetry reaches zero even if the position of the target and beam is shifted. This happens because effects caused by beam positioning and the existence of the target nullify each other. According to the data obtained, the closer the row is to Z axis, the earlier its spectrum reaches this point which has its geometrical explanation.

When there is no vacuum modules measured, asymmetry is almost -0.15 for each row and the farther the row is from the center, the later it reaches zero asymmetry (The left side of Figure 6.6).

In case when vacuum modules are turned on, asymmetry between outer crystals (Appendix 8.1) is more (approximately -0.2) than for inner ones (almost -0.15) if the vertical position of the beam-target system is zero.

When the beam-target vertical coordinate is maximum (10mm), the measured asymmetry decreases constanly from 0.15 to 0 if we move from inner crystals to outer ones. But this is true only for the first three rows (Appendix 8.1). The asymmetry between crystals in the fourth row is 0.05 when the vertical shift is maximum. It has the same reason as in case of Section 6.1, when vacuum modules are turned on. The asymmetry increases due to varied interaction of particles with different sides of symmetric modules when a beam is shifted.

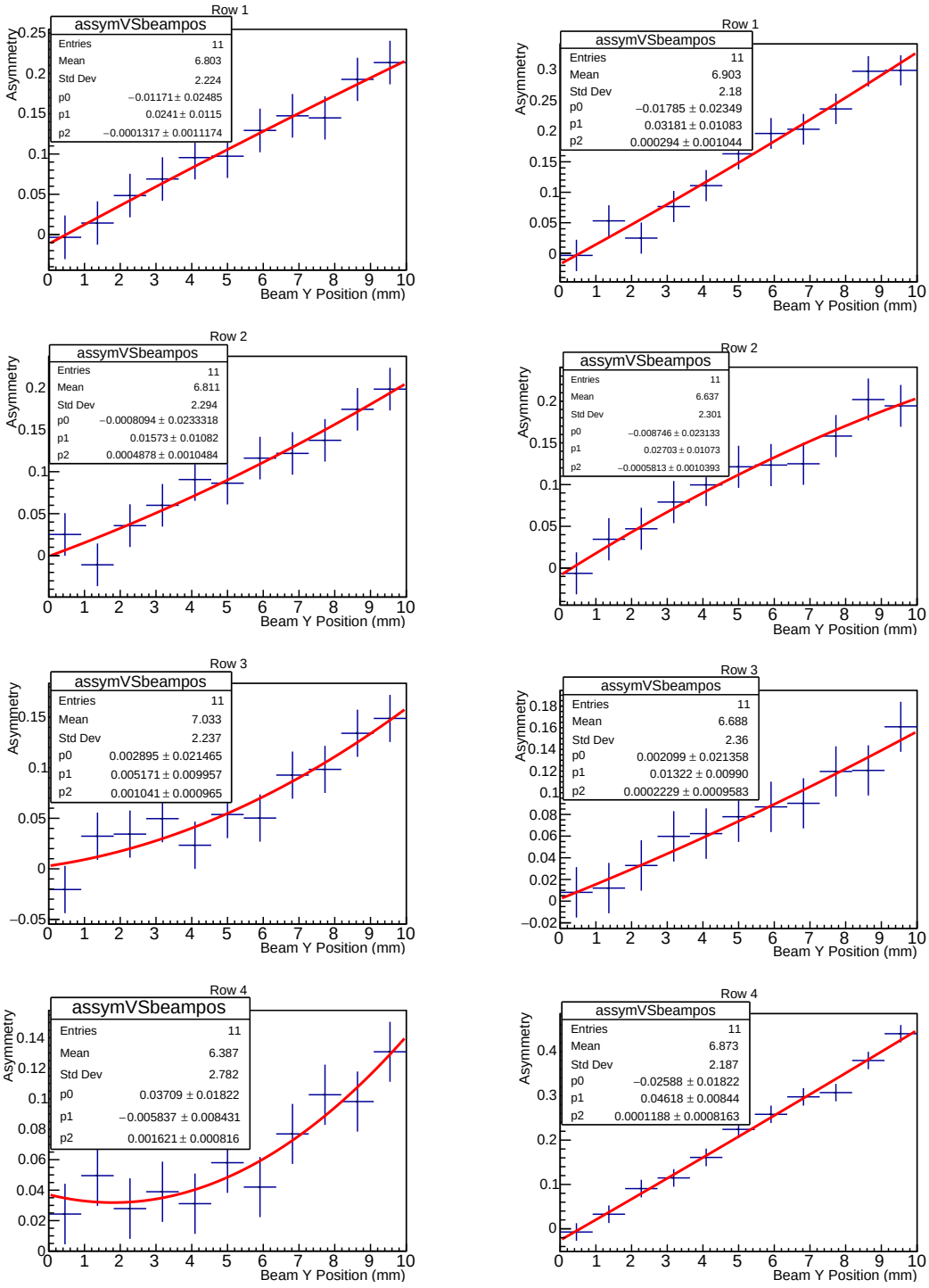

(a) Vacuum Modules OFF

(b) Vacuum Modules ON

Figure 6.4: Dependence of ssymmetry on a beam vertical position.

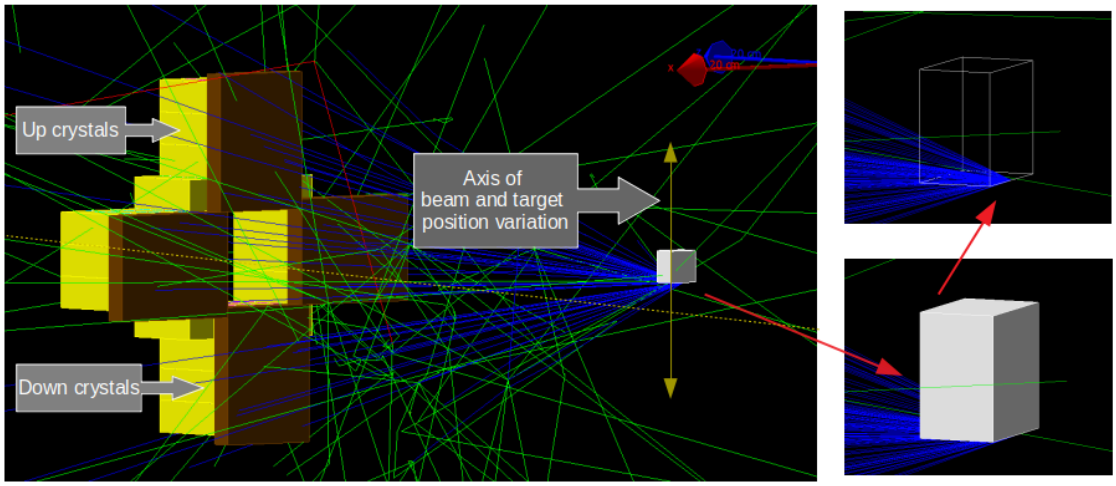

Figure 6.5: Beam and target positioning

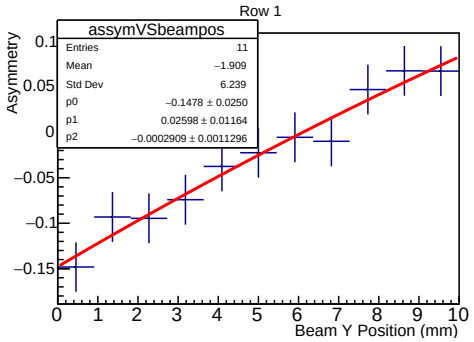

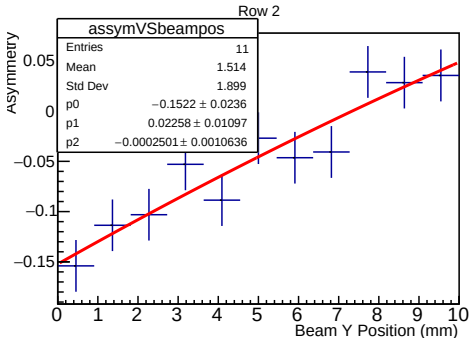

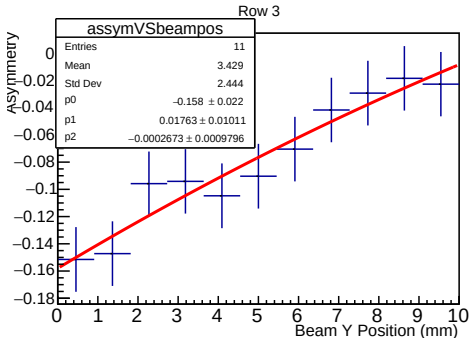

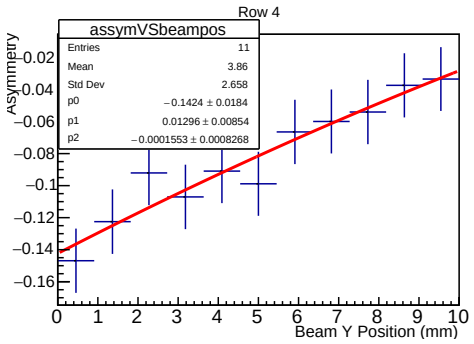

(a) Vacuum Modules OFF

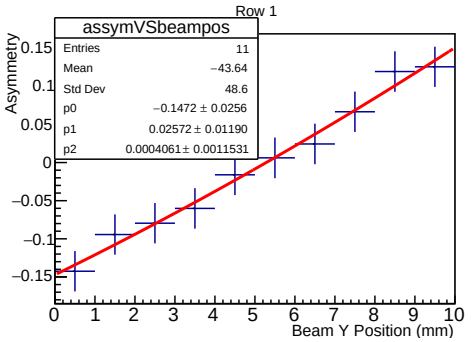

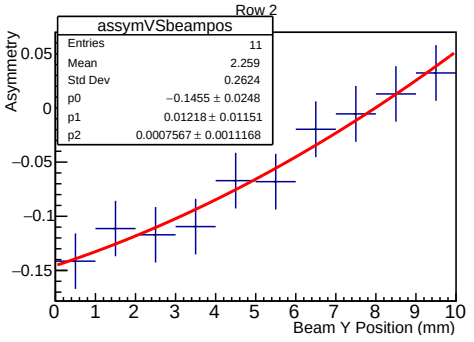

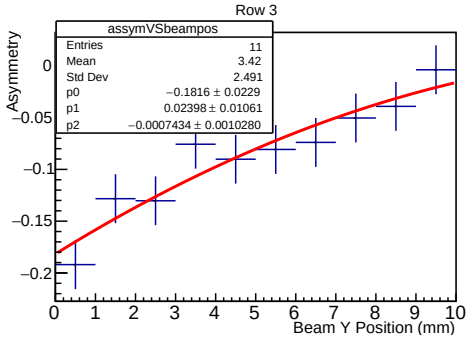

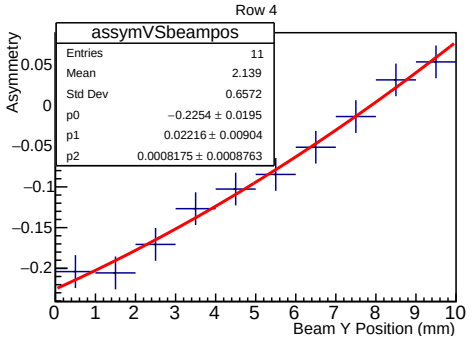

(b) Vacuum Modules ON

Figure 6.6: Dependence of symmetry on the beam-target vertical position.

Chapter 7

Summary

In this thesis, we addressed to the problem of the Monte Carlo simulation code modification for the JEDI polarimeter. In the last few years the Polarimeter detector was partially built and the final version is developing. The modules of the calorimeter, some mechanical parts and other principal components were assembled. The existing simulation software had to be updated in order to study the polarimeter performance in its current state. The following developments, modifications, and analysis were done:

- The polarimeter geometry has been modified according to the existing configuration. The geometry components were modified.

    1. The geometry of the calorimeter modules, based on the LYSO crystals and SiPM photodetectors was created.
    2. The storage ring vacuum pipe was modified in a modular structure in a shape it was recently built and assembled.
    3. A ring plastic scintillator, located in front of the LYSO crystals, was replaced by four rectangular scintillators, as it is done in real test measurements. The scintillator geometry was designed in a way that allows to have the unit of arbitrary shape.
    4. The test target also may have certain effect on asymmetry so its positioning and shape was also optimised from disc like structure to a box shape with dimensions $30 \times 30 \times 20\, mm^3$. The shape and placement of the target is extremely important in testing its affect on the circulating beam.

- Another important aspect of the simulation code is the particles' generator and their interactions with environment materials mainly with the vacuum pipe components.

1. The interaction generator for the block target was developed. The block target produced asymmetric events (of dC elastic scattering) on the calorimeter. We estimated the asymmetry in various target positioning.
2. The interaction generator was modified in order to generate elastic or inelastic dC interaction, including the interaction with polarized beam. Also, some nonphysical interaction generators were added for technical purposes (e.g. with uniform polar distribution).
3. Another problem was to investigate influence of the target material and position on forming the load asymmetry. The box shape carbon target of different thicknesses was used to test its effects and different horizontal positions with respect to the beam were tested.
4. The azymutal and the polar angles were considered as random variables and the differential cross section shape and the polarization can be implemented by a user for different materials.

- As it is described above, the beam in the previous version of the simulation code had non-zero transverse dimensions. The particles were generated randomly in a circle of radius $3\,mm$ and all particles had the momenta directed along Z axis. In the updated simulation code the particle generator is defined so that it is posible to polarize the beam though the point where particles formation is always the same for one beam. In the code's current version it is possible to alter any beam parameter.

- The updated simulation code for the polarimeter firstly was tested for several different cases. The first problem was to estimate the uncertainty caused by the simulation itself to check how properly it worked. It was concluded that uncertainties due to numerical calculations do not exceed the statistical error of asymmetry.

- The influence of the beam vertical position on the measured asymmetry was investigated. It means that asymmetry was calculated for several different vertical positions of the beam. We tested the beam and the target in such a position that the interaction was creating inhomogeneity in the vertical direction.

- The influence of the vacuum modules on the measured asymmetry has been studied.

    1. Six independent modules of the beam pipe has been used separately in the simulation. The fake asymmetry induced by the symmetric beam is 0 in the uncertainty limits.

2. Completely assembled vacuum beam pipe also does not produce significant background an a fake asymmetry.
3. The simulation has been performed using the existing calorimeter setup for different beam and target positioning, such as: beam is located at fixed point for low thickness target, at back axit point for box target and inside the box target at different depths.
4. The most important conclusion is the following: all existing parts of the polarimeter including the calorimeter and the test target unit do not produce the fake asymmetry. The conclusion is made with average uncertainty of 0.03.

- The modular structure of the updated simulation code makes possible to modify geometry and/or interaction generator classes. It can be used for future study of the polarimeter performance by updating the set-up to its final shape.

The idea of creating the simulation was generated by the fact that all results gained from it corresponds to the ones obtained from a real experiment. Within this Master Thesis several models and situations which might happen in a real experiment are considered and their results are predicted using the numerical methods.

Chapter 8

Appendices

8.1 Appendix 1

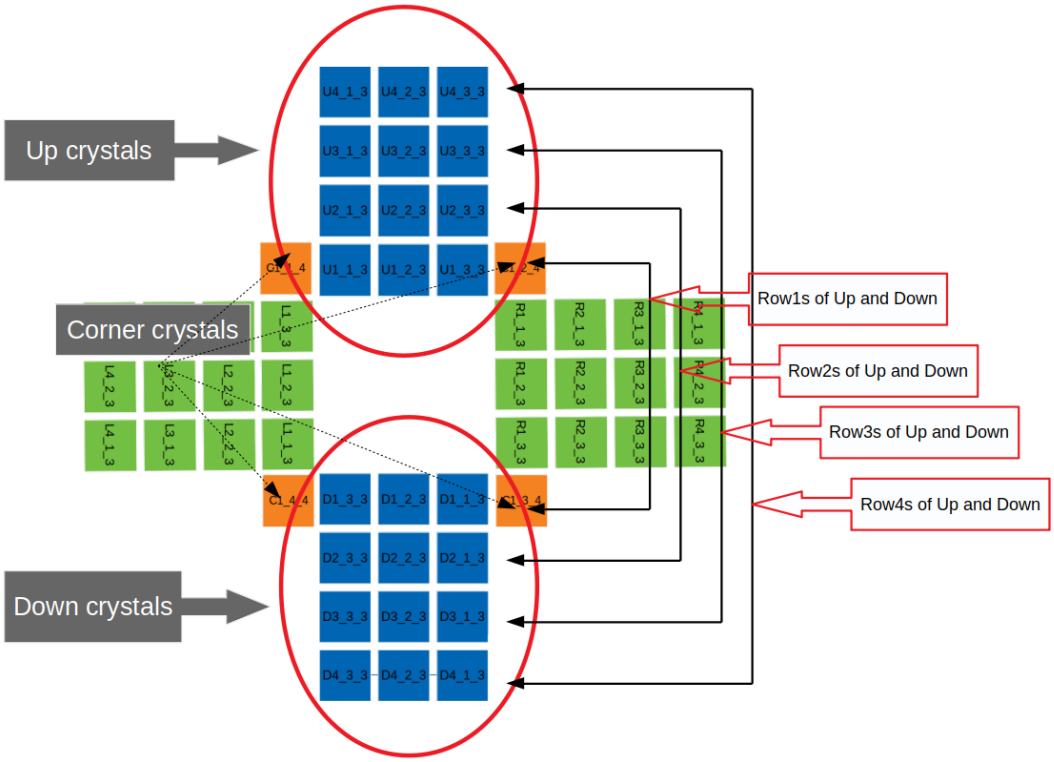

Figure 8.1: Grouping crystals

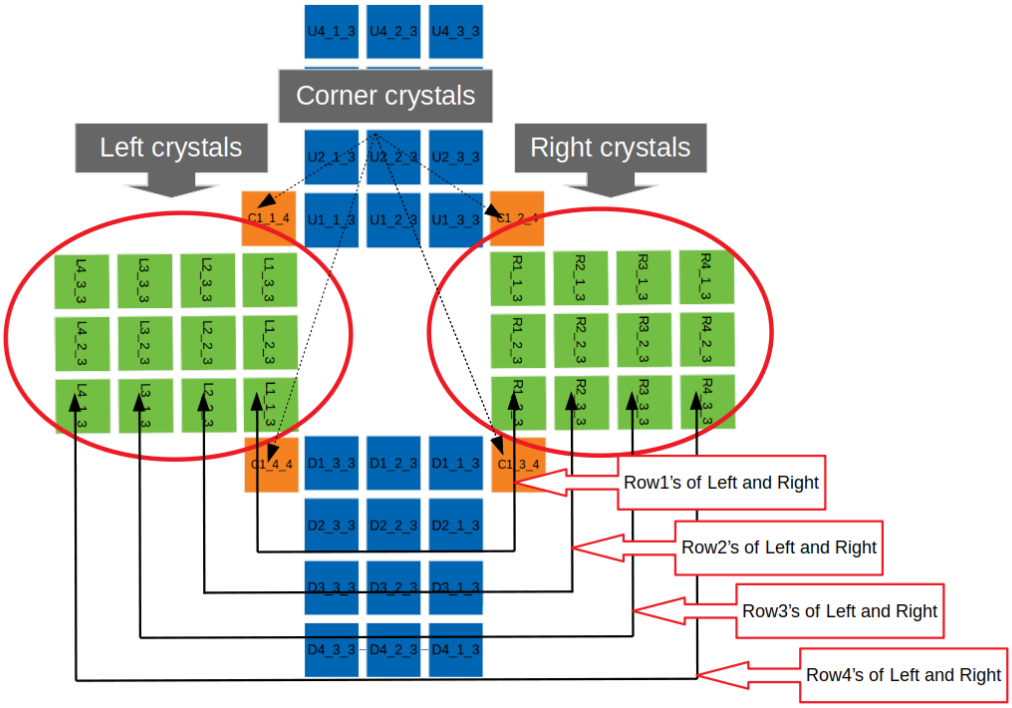

Figure 8.2: Grouping crystals

8.2 Appendix 2

There are several kinds of histograms in the aforementioned Master Thesis in which physical parameters and results of the measurements are described.

The first kind of histogram designates energy transferred to particular LYSO modules and asymmetry. There are two histograms in Figure 8.3. The left one comprises information regarding the number of particles detected by Left and Right LYSO crystals (Appendix 8.1) and the right histogram shows asymmetry.

The asymmetry displayed on the histogram on the right side is counted by the formula:

$$A_y = \frac{N_L - N_R}{N_L + N_R} \tag{8.1}$$

where N_L is the sum of particles with kinetic energy between 200MeV and 300MeV identified by one Row (Appendix 8.1) of Left crystals and N_R is the sum of particles sensed by one Row of Right crystals.

It is worth noting that the same principle is valid for Up and Down crystals.

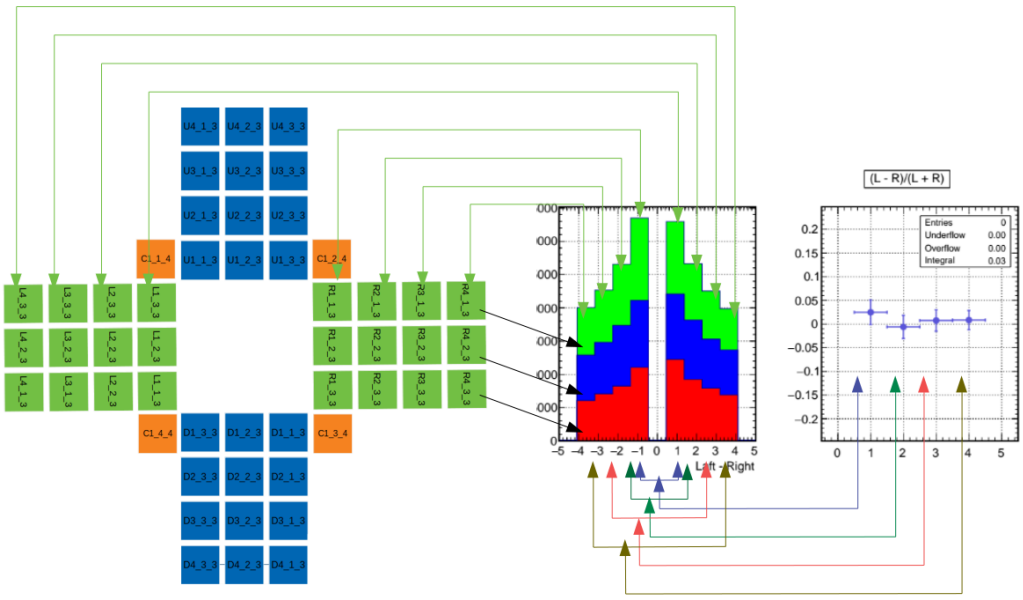

Figure 8.3: The histograms visualizing asymmetry.

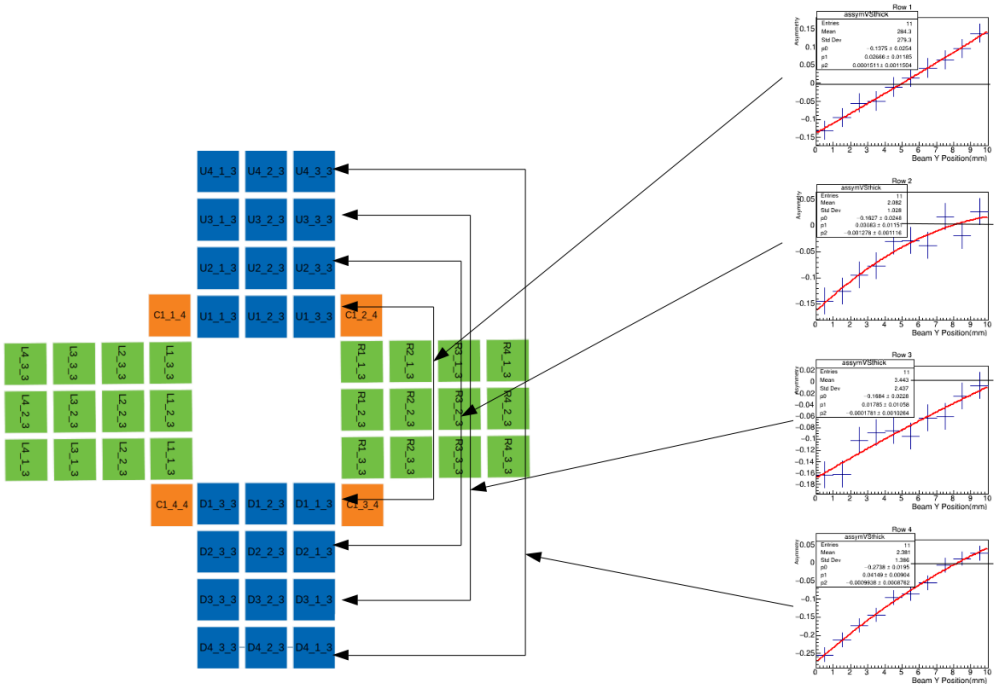

Figure 8.4: The histograms visualizing asymmetry between Up and Down crystals when the beam's vertical position is different from zero.

Another type of histograms which is also crucial is the one which reflects asymmetry between Up and Down crystals when the beam Y position is altered.

This type of histograms is illustrated in Figure 8.4. The first histogram with the label "Row 1" expresses asymmetry between first rows of Up-Down crystals (Appendix 8.1). On the horizontal axis the Y coordinate of a beam is marked, while the asymmetry is indicated on its vertical exis. Asymmetry is calculated by the aquation 9.1.

8.3 Appendix 3

The purpose of Chapter 6 is to observe the influence of beam Y coordinate on forming the ultimate asymmetry when the target material is turned on and off. In order to exclude errors caused by the geometry of detector and beam parameters, the validity of the simulation for maximum and minimum Y coordinates of a beam should be checked in a graphic mode.

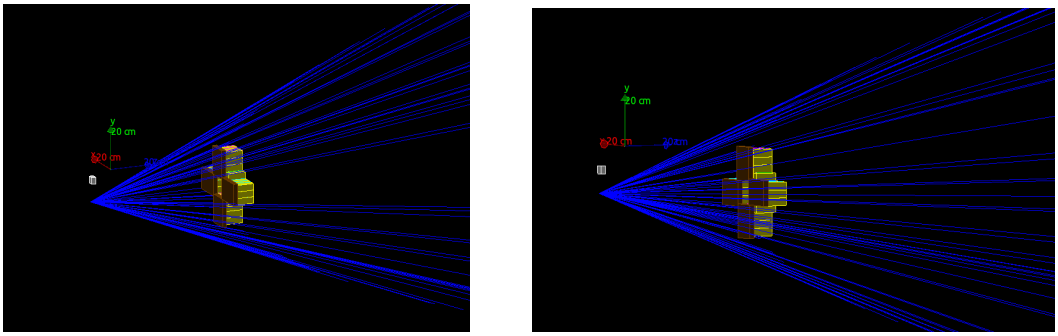

(a) Geometry (b) Geometry

Figure 8.5: (a) and (b) displays that a beam with null and maximum vertical coordinates respectively will cover the detector surface.

As mentioned in Section 3.4, particles' momenta direction has a distribution which is a function of ϕ and θ. In addition, ϕ angle has a certain range, which originally was defined from 3 to 22 degrees.

In Figure 8.5(a) Y coordinate of a beam is zero and in Figure 8.5(b) its Y coordinate is 20mm. It is apparent that upper limit of ϕ is so large that a beam of particles cover the whole surface of detector acceptance.

On the other hand, the lower limit of ϕ should meet the following conditions: None of the particles shot in this direction should interact with crystals even if the beam's vertical coordinate is maximum. This condition ensures the precision of spectra of inner crystals.

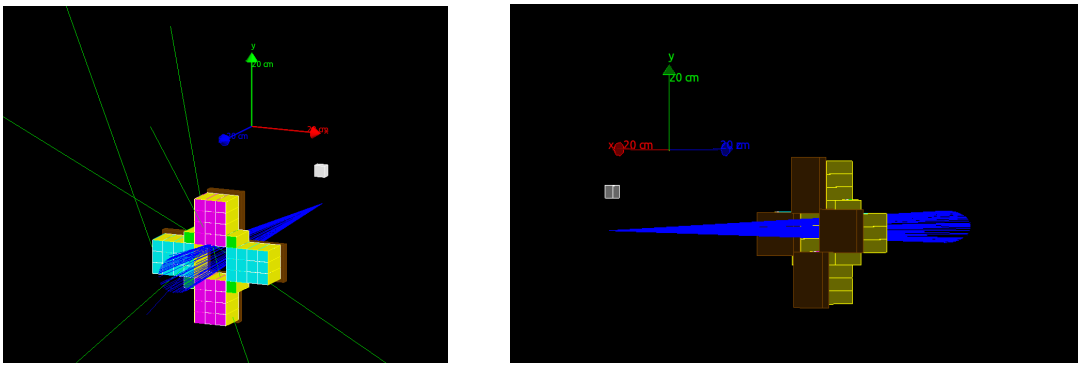

(a) Geometry (b) Geometry

Figure 8.6: (a) elucidates interaction between a beam of particles and crystals when $\phi = 3^o$ while (b) explains the one when $\phi = 2^o$. In both cases the beam has maximum (10mm) vertical position.

It is palpable from Figure 8.6 that if $\phi = 3^o$ and the beam's vertical position is maximum, some particles interact with LYSO crystals (the output of this interaction is marked with green lines), therefore the lower limit of ϕ is decreased to 2^o.

8.4 Appendix 4

It is assumed that the error of entire number of particles signalled by one crystal, each of which has defined energy, is square root of itself.

$$\delta N_{1,2} = \sqrt{N_{1,2}} \tag{8.2}$$

Where N_1 and N_2 are energies conveyed to oppositely arranged crystals and asymmetry is calculated by the formula:

$$A = \frac{N_1 - N_2}{N_1 + N_2} \tag{8.3}$$

where A is the asymmetry explained in Appendix 8.2.
To measure uncertainty,

$$\delta f(N_1, N_2) = \sqrt{(\frac{\partial f}{\partial N_1})^2 \delta N_1^2 + (\frac{\partial f}{\partial N_2})^2 \delta N_2^2} \tag{8.4}$$

More precisely,

$$\frac{\partial f}{\partial N_1} = 2\frac{N_2}{(N_1 + N_2)^2} \tag{8.5}$$

$$\frac{\partial f}{\partial N_2} = 2\frac{N_1}{(N_1+N_2)^2} \tag{8.6}$$

Eventually,

$$\delta f(N_1, N_2) = \frac{2N_1N_2}{(N_1+N_2)^2}(\sqrt{\frac{1}{N_2}+\frac{1}{N_1}}) \tag{8.7}$$

8.5 Appendix 5

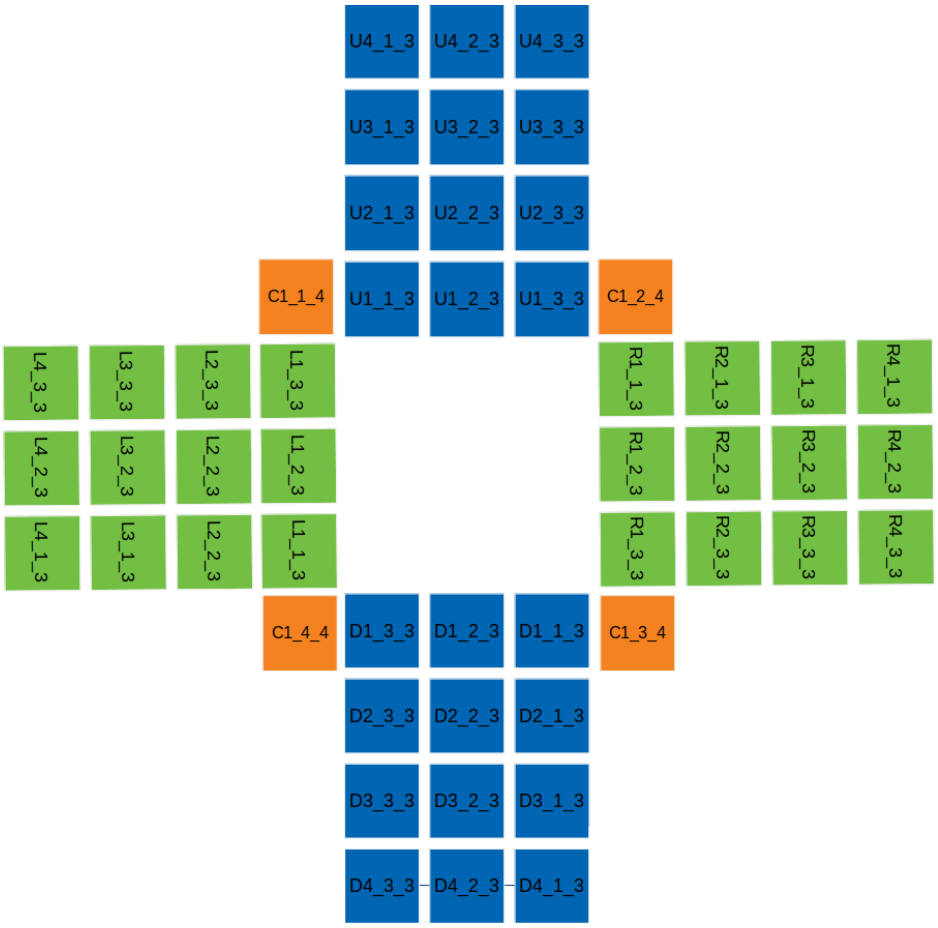

Figure 8.7: Detectors setup with their names.

Bibliography

[1] Aaij R., Abellan Beteta C., Adeva B. et al. (2012). *Evidence for CP Violation in Time-Integrated $D_0 \to h^- h^+$ Decay Rates*. Phys. Rev.Lett.,108,111602.

[2] M. S. Sozzi. *Discrete Symmetries and CP Violation*. 1 edition, 2008.

[3] A. Riotto, M. Trodden. *Recent progress in baryogenesis*, Annu. Rev. Nucl. Part. S 49 (1) (1999) 35–75, http://dx.doi.org/10.1146/annurev.nucl.49.1.35.

[4] Lüders G. (1954). *On the Equivalence of Invariance under Time-Reversal and under Particle-Antiparticle Conjugation for Relativis-tic Field Theories*. Kongelige Danske Videnskabernes Selskab,Matematisk-Fysiske Meddelelser.,28,1-17.

[5] Maier R. (1997). *Cooler synchrotron COSY-Performance and per-spectives*, Nuclear Instruments and Methods in Physics Research Section A: Accelerators, Spectrometers, Detectors and Associated Equipment,390,1-8.

[6] W. Dekens, J. de Vries, J. Bsaisou, et al. *Unravelling models of CP violation through electric dipole moments of light nuclei*. JHEP, 07:069, 2014.

[7] W. Dekens, J. Vries, J. Bsaisou, W. Bernreuther, C. Hanhart, U.-G. Meißner, A. Nogga, A. Wirzba, *Unravelling models of CP violation through electric dipole moments of light nuclei*, J. High Energy Phys. 2014 7 (2014) 1–57, http://dx.doi. org/10.1007/JHEP07(2014)069.

[8] Baker C et al. 2007 Phys.Rev.Lett. 98 149102 (Preprint 0704.1354)

[9] See http://collaborations.fz-juelich.de/ikp/jedi for Jülich Electric Dipole moment Investigations

[10] F. Rathmann and N. Nikolaev. *Precursor experiments to search for permanent electric dipole moments (EDMs) of protons and deuterons at COSY* in 8th International Conference on Nuclear Physics at Storage Rings (STORI11), PoS STORI11 (2011) 029, 2011.

[11] *Review of Particle Physics*. EPJ, C 15 (2000)

[12] F. Müller. *Polarimeter Development for Electric Dipole Moment Measurements in Storage Rings*. 2019.

[13] F. J. M. Farley, K. Jungmann, J. P. Miller, W. M. Morse, Y. F. Orlov, B. L. Roberts, Y. K. Semertzidis, A. Silenko, and E. J. Stephenson. *New Method of Measuring Electric Dipole Moments in Storage Rings*, Phys. Rev. Lett. 93, 052001 (2004).

[14] Y. K. Semertzidis, *The status of the storage ring EDM experiment*, AIP Conf. Proc. 1182, 730 (2009).

[15] Z. Bagdasarian, et al., *Measuring the polarization of a rapidly precessing deuteron beam* PHYSICAL REVIEW SPECIAL TOPICS - ACCELERATORS AND BEAMS 17, 052803 (2014)
http://collaborations.fz-juelich.de/ikp/jedi/public_files/colpapers/bagdasarian.pdf

[16] C. A. Baker. Phys. Rev. Lett. 97 (2006) 131801 [arXiv:hep-ex/0602020].
http://collaborations.fz-juelich.de/ikp/jedi/public_files/indpapers/0911.3981v2.pdf

[17] The Storage Ring EDM Collaboration. *A Proposal to Measure the Proton ElectricDipole Moment with 10^{-29} e·cm Sensitivity*. March 2011.

[18] G. Guidoboni, at all, *How to Reach a Thousand-Second in-Plane Polarization Lifetime with 0.97-GeV=c Deuterons in a Storage Ring* Phys. Rev. Lett. PRL 117, 054801 (2016)

[19] Geant4 Collaboration. *Geant4 User's Guide for Application Developers*. 2016.
http://geant4.web.cern.ch/geant4/

[20] J. Allison. *Nuclear Physics News*. 17, 2 (2007). http://root.cern.ch.

[21] Y. Satou. et al., *Phys.Lett.* B 549 (2002) 307.

[22] L. Canetti, M. Drewes, and M. Shaposhnikov. *Matter and Antimat-ter in the Universe.* New Journal of Physics, Focus Issue on the Origin of Matter,Vol. 14 (095012), 2012.

[23] F. Trinkel. *Development of a Rogowski coil Beam Position Monitor for Electric Dipole Moment measurements at storage rings*. 2017.

[24] M. Zurek. *Search for Electric Dipole Moment (EDM) at a Storage Ring With JEDI*. 2018.
http://collaborations.fz-juelich.de/ikp/jedi/documents/talks.shtml

[25] J.S. Slim. *A Novel Waveguide RF Wien Filter for Electric Dipole Moment Measurements of Deuterons and Protons at the COolerSYnchrotron (COSY)/Juelich*. 2018.

[26] F. Hinder. *Development of Beam Diagnostic Systems for Electric Dipole Moment Measurements at Particle Accelerators*.

[27] M. Zurek. *Polarimetry for a Storage-Ring Electric-Dipole-Moment Measurement*. 2018.
http://collaborations.fz-juelich.de/ikp/jedi/documents/talks.shtml

[28] G. Guidoboni. *Spin Coherence Time studies for the storage ring EDM search*. 2010-2012.

[29] A. Pesce. *Spin Tracking Studies for EDM Searchin Storage Rings*. 2011/2013.

[30] E.V. Valetov. *Field Modeling, Symplestic Tracking, and spin Decoherence for EDM and Muong-2 Lattices*. 2017.

[31] S. Chekmenev. *Investigation of Possibilities to Measure the Deuteron Electric Dipole Momentat storage rings*. 2017.

[32] M.S. Rosenthal. *Experimental Benchmarking of Spin Tracking Algorithms for Electric Dipole Moment Searches at the Cooler Synchrotron COSY*. 2016.

[33] J. Slim, R. Gebel, D. Heberling, F. Hinder, D. Hölscher, A. Lehrach, B. Lorentz, S. Mey, A. Nass, F. Rathmann, L. Reifferscheidt, H. Soltner, H. Straatmann, F. Trinkel, J. Wolters. *Electromagnetic Simulation and Design of a Novel Waveguide RF Wien Filter for Electric Dipole Moment Measurements of Protons and Deuterons* http://collaborations.fz-juelich.de/ikp/jedi/public_files/indpapers/RF-Wien-Filter_NIM-A_2016.pdf

[34] A. Magiera. *Control of systematic uncertainties in the storage ring search for an electric dipole moment by measuring the electric quadrupole moment* PHYSICAL REVIEW ACCELERATORS AND BEAMS 20, 094001 (2017)
http://collaborations.fz-juelich.de/ikp/jedi/private_files/indpapers/prab-20-094001-2017.pdf

Chapter 9

Acknowledgements

Firstly, I wish to thank my sipervisors Dr. Irakli Keshelashvili (The Institute of Nuclear Physics, Juelich, Germany. E-mail - i.keshelashvili@fz-juelich.de), Prof. Dr. Zaza Metreveli (The Agricultural University of Georgia, Georgia. E-mail - z.metreveli@agruni.edu.ge), to whom I am particularly grateful for all their unprecedented guidance, crucial instructions and considerable consultancy at all stages of the work, and Prof. Giorgi Jorjadze (The Free University of Tbilisi, Georgia - E-mail - g.jorjadze@freeuni.edu.ge), under whose supervision I have graduated from my Bachelor and Master programs.

The Master Thesis was performed at the Institute of Nuclear Physics (IKP) of the Forschungszentrum Juelich (Germany). The internship was funded by Ivane Javakhishvili Tbilisi State University SMART—EDM Laboratory (Dr. David Mchedlishvili) and the Institute of Nuclear Physics at Juelich (Germany).

Moreover, I would like to thank the Director of IKP - Prof. Dr. Hans Stroeher and express my deep appreciation to Dr. Andro Kacharava for his valuable assistance with my study trips. Most importantly, I am more than willing to specially convey my considerable gratitude to Prof. Dr. Giorgi Macharashvili from Tbilisi State University for his key role in the fulfillment of my Master Thesis.

Last but not least, I am pleased to acknowledge the work performed by my co-workers whose works and measurements were used in order to effectively eccomplish my Master Thesis (Dr. David Mchedlishvili, PHD students - Fabian Mueller and Otar Javakhishvili, Dr. Mirian Tabidze, Michael Gagoshidze).